Università degli studi di Padova

Dipartimento di Ingegneria Industriale

Corso di Laurea Magistrale in Ingegneria dell'Energia Elettrica

Impact of VSC converters fault current injection on Incremental Quantities based distance protections

Relatore:
Prof. Roberto Turri
Correlatore:
Joachim Vermunicht

Laureando:
Lorenzo Feletto

Anno Accademico 2023/2024

Abstract

Renewable energy sources (RES) and high-voltage direct current (HVDC) links are interfaced to the grid using power electronic converters (PECs). Unlike traditional synchronous generators, PECs fault behaviour is fully controlled and needs to satisfy grid code requirements. This regulated fault current behaviour presents significant challenges to protection schemes. Incremental Quantities (IQ) line protections are a type of time domain protections. These protections are advantageous because they can respond to faults more quickly than traditional phasor-based distance protections. Faster fault clearing enhances system stability and reliability and improves power quality. An example of such a protection scheme is the TD21 distance protection element, implemented in the commercial SEL-T400L relay.

The objective of this thesis is to analyse the impact of fault current injection by voltage source converters (VSCs) on the TD21 distance protection element. To achieve this, several tasks were undertaken: a literature review on the fault behaviour of PECs, the implementation of a VSC model in MATLAB/Simulink, a review of incremental quantities-based protections, and the implementation of the TD21 element in MATLAB/Simulink.

Simulation results reveal that the VSC's fault current affects the performance of the TD21 distance protection element. The reduced fault current provided by the VSC can hinder the protection element's ability to detect in-zone faults effectively. Additionally, the irregular fault current during the VSC's transient response can lead to incorrect operation of the protection element for faults outside the protected zone.

Acknowledgments

I would like to express my sincere gratitude to several individuals and groups who have supported me throughout this journey.
First, I want to thank my supervisor, Prof. Roberto Turri, for his encouragement and assistance in helping me complete this thesis.
I also want to thank my co-supervisor, Joachim Vermunicht, who guided and assisted me in starting this thesis during my period of study in Belgium. His mentorship and support have been greatly appreciated.
I am deeply grateful to my family, especially my parents, Graziella and Franco, for their hard work and unwavering support. Their dedication and belief in me have been a constant source of motivation.
Lastly, I want to thank my friends who have stood by me during this chapter of my life. Your companionship and encouragement have made this journey more meaningful and enjoyable.

Thank you all for your support and for believing in me.

Contents

Acronyms

dq0 Direct Quadrature Zero

FCI Fault Current Injection

FFCI Fast Fault Current Injection

FRT Fault Ride Through

ICC Inner Current Controller

IQ Incremental Quantities

OPC Outer Power Controller

PEC Power Electronic Converters

PLL Phase Locked Loop

PWM Pulse Width Modulation

SIR Source Impedance Ratio

SRF Synchronous Reference Frame

VSC Voltage Source Converter

1 Introduction

1.1 Background

Power systems are undergoing significant transformations due to the increased integration of renewable energy sources (RES) and high-voltage direct current (HVDC) links, which are gradually replacing synchronous generators [27]. RES and HVDC links employ power electronic converters (PECs) to deliver power to the grid. Among these converters, voltage source converters (VSCs) are the predominant technology used in HVDC applications and for interfacing RES. Unlike synchronous generators that inherently inject fault currents during faults, PECs regulate their fault current injection based on grid code requirements, fault type, and operating conditions. This behaviour of PECs poses challenges to distance protection schemes.

The impact of fault currents from PECs on traditional distance protection schemes has been already studied in the literature [10] [26] [11]. This thesis aims to analyse the impact on time-domain distance protections, specifically those based on incremental quantities (IQ). Incremental quantities based protections operate by detecting sudden changes in voltage and current that occur during a fault. These protections are advantageous because they can respond to faults more quickly than traditional methods, which rely on fundamental frequency components (phasors) [19]. By analysing the immediate transient response of the system to a fault, incremental quantities based protections can reduce fault detection and clearance times significantly. Faster fault clearing not only enhances system stability and reliability but also minimizes damage to equipment and improves power quality.

1.2 Objective and limitations

This thesis aimes to analyze the impact of fault current injection by power electronic converters (PECs), specifically VSCs, on incremental quantities based protection, specifically the TD21 distance protection. To achieve this, several key tasks were undertaken:

- **Literature review on fault behavior of PECs:** The purpose was to compare the behavior of PECs with traditional generators to highlight potential repercussions on protection systems; and to analyze grid codes to understand the requirements imposed on PECs.
- **Implementation of a VSC converter in MATLAB/Simulink:** A model capable of operating under both normal and fault conditions, following the requirements of grid codes.
- **Literature review on Incremental Quantities based protection:** To understand the techniques and operating principles behind this type

of protection, particularly for the TD21.

- **Implementation of the TD21 Distance Protection Element in MATLAB/Simulink:** A model based on scientific articles, subsequently tested and validated.

These tasks were necessary to achieve the final objective: evaluate the influence of the fault behaviour of the implemented VSC on the implemented TD21 element, through a simulation in MATLAB/Simulink.

Limitations of this work include:

- Incomplete parameters and settings: Potential gaps exist in specific parameters and settings of the TD21 model due to incomplete information in the literature and manuals. Despite these limitations, the implemented model performed as expected, confirming the validity of the obtained results.
- Simplified VSC model: The VSC model is not very detailed, also some simplifications have been adopted (constant DC voltage source). These are permissible since the focus of this thesis concerns fault behaviour, which is minimally influenced by these simplifications and lack of details.
- Simplified element models: The transmission line was modelled as a simple RL impedance, omitting more complex network configurations and effects such as capacitance and mutual coupling.
- Three-phase fault simulation: The study focused exclusively on symmetric three-phase faults. Real-world scenarios involving asymmetrical faults and other complex fault types were not considered in this analysis.

These simplifications allowed for an initial assessment. More detailed scenarios could be explored in future work, using this study as a foundational reference.

1.3 Outline

This thesis is structured in six chapters. In Chapter 2, the behavior of Power Electronic Converters (PECs) during faults is described and compared to that of traditional generators. Additionally, the requirements imposed by grid codes on PECs are discussed. In Chapter 3, the implemented VSC model is explained, detailing its control structure and components. Simulations performed under both normal operating conditions and fault conditions are also described. Chapter 4 is dedicated to the TD21. The concept of incremental quantities is explained, the operation of the TD21 is described, and the criteria used for testing along with the simulations performed to validate the model are presented. In Chapter 5, the combined simulations of the implemented TD21 and VSC and the results obtained are described. In Chapter 6, conclusions and recommendations for future work are presented.

2 Fault Behaviour of Power Electronic Converters

Power electronic converters (PECs) exhibit distinct behaviour during faults compared to traditional synchronous generators. Unlike synchronous generators, which inherently generate fault currents, converters can control their output current, providing a predefined fault current injection. This characteristic is critical for grid stability and protection schemes.

The fault behaviour of synchronous generators is well defined: when a fault occurs they will respond as an ideal voltage source behind an impedance (classified according to the fault period: sub-transient, transient or steady state) and inject fault currents up to 5-10 pu [6]. Their short circuit current can be divided into two components: a transient component (decaying exponential) and a sinusoidal steady state component.

By contrast, the fault response of PECs is determined by their control system. Moreover, their fault current contribution is limited. That is because the semiconductor switches of the converters cannot withstand high overload currents. To protect these switches from thermal overload and hence destruction, the control system must actively limit the fault current. From the literature, it can be concluded that the steady state fault current contribution of PECs is limited to 1-1,2 pu [6]. Designing the switches for higher currents results in significantly higher costs.

In conclusion, power electronic converters behave as a controlled current source under fault conditions, and their specific fault behaviour is dictated by grid codes.

2.1 Grid Code Requirements

In 2016, the EU Commission released two network codes: the Network Code on Requirements for Generators (NC RfG) [2] and the Network Code on High Voltage Direct Current Connections (NC HVDC) [1]. These regulations define network codes specifying the criteria for connecting power-generating facilities (in the case of NC RfG) and high-voltage direct current (HVDC) systems and DC-connected power park modules (in the case of NC HVDC) to the grid.

These network codes provide two key definitions regarding the fault behaviour of PECs: Fault ride through (FRT) and Fast fault current injection (FFCI).

"Fault ride through means the capability of electrical devices to be able to

remain connected to the network and operate through periods of low voltage at the connection point caused by secured faults" [2].

"Fast fault current means a current injected by a power park module or HVDC system during and after a voltage deviation caused by an electrical fault with the aim of identifying a fault by network protection systems at the initial stage of the fault, supporting system voltage retention at a later stage of the fault and system voltage restoration after fault clearance" [2].

FRT implies that a device should have the capability to remain connected to the grid during temporarily low voltages at the connection point. The FRT capability is specified with a voltage-time curve. The curve shows when the PEC is allowed to disconnect.

In practice, the concept of FFCI means injecting current, predominantly reactive according to most grid codes, based on the voltage drop across the PEC. For this reason, it is often referred to as Reactive Current Injection (RCI). Some grid codes define a no-injection zone (deadband): if the voltage is within this band, the PEC should not inject current. Figure 1 shows the characteristics of the FFCI, where the factor k determines how quickly the maximum injectable current i_{max} is reached.

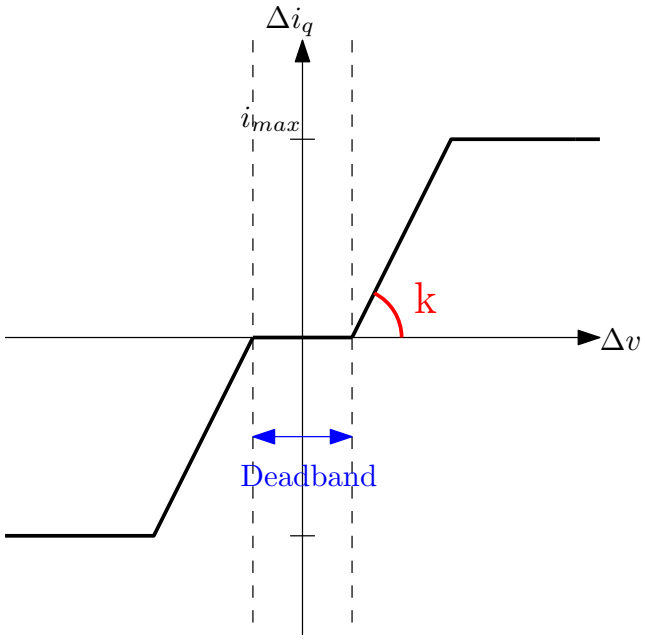

Figure 1: FFCI according to grid codes

In the NC RfG and NC HVDC much freedom has been given at national

level to specify the requirements related to FFCI and FRT. Consequently, there is variation in the existing FFCI and FRT requirements among European countries. A comparison of national implementation of requirements on FFCI is reported in [13] (one of the deliverables produced by the MIGRATE project [4]).
The adopted approach is the same; the few differences are found in the definitions of the involved quantities and the parameters used. These limited disparities allow overlapping of the adopted strategies. Therefore, the choice to follow the guidelines of one network code over another does not impact the analysis conducted in this thesis.

The decision was made to follow the directives of the German network code, as it was one of the first to provide specific indications regarding FFCI requirements (dating back to at least 2007 [8]).

2.1.1 German Implementation of the FFCI Requirements

In Table 1 the main features of the German implementation of the FFCI requirements are listed.

Activation requirement of the fault current's injection mode	$V_{LL} > 1.1 \cdot V_n \quad \text{or} \quad V_{LL} < 0.9 \cdot V_n$
Additional reactive current during balanced faults	$\frac{\Delta I_q}{I_n} = k \cdot \frac{V_f - V_{pf}}{\frac{V_n}{\sqrt{3}}}$
Adjustment range for k	$2 \leq k \leq 6$
Default value for k	$k = 5$
Rise time and Settling time of the fault current contribution [ms]	$T_r \leq 30 \quad T_s \leq 60$
Priority between active and reactive current during faults	Reactive current

Table 1: German Implementation of the FFCI Requirements [13]

The variables used in Table 1 are also listed below:

- V_{LL}: line to line voltage

- V_n: rated voltage
- ΔI_q: additional reactive current during balanced faults
- I_n: rated current
- V_f: voltage during fault
- V_{pf}: pre-fault voltage

2.1.2 Negative Sequence Current Injection

In some grid codes, specific requirements are outlined for the injection of negative sequence current. Negative sequence current injection is usefull for the detection and management of unbalanced faults, as it helps in identifying and mitigating asymmetrical conditions in the power system. This type of current injection assists in maintaining system stability and ensuring the proper functioning of protection schemes during unbalanced fault conditions.

However, the scope of this thesis is limited to the analysis of symmetrical three-phase faults. Consequently, the requirements and implementation details for negative sequence current injection are not considered in this work. Future studies can explore the impact and design of negative sequence current injection mechanisms to provide a comprehensive understanding of PEC behavior under various fault conditions, including unbalanced faults.

3 VSC Model

3.1 Control of the VSC

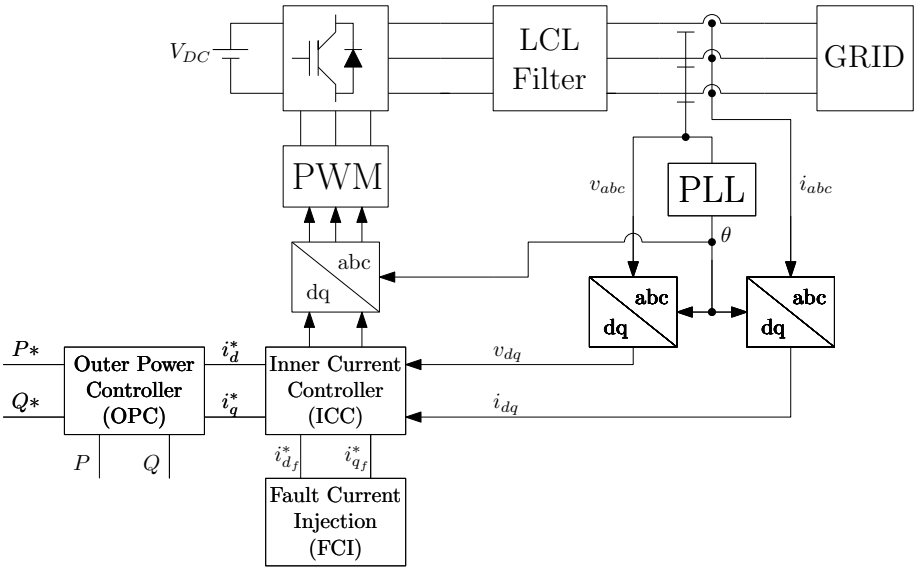

Figure 2: Structure of the converter control

The implemented Voltage Source Converter (VSC) utilizes the Pulse-Width Modulation (PWM) scheme and is controlled with Proportional-Integral (PI) controllers in the dq0 reference frame. Working in the dq0 reference frame enables the decoupling of the AC quantities into DC components, allowing the use of PI controllers for control. The PI controllers are tuned to ensure optimal performance and stability of the VSC.

The block diagram of the VSC is illustrated in Figure 2, the control structure of the converter is composed of the following components:

- DC-link
- LCL filter: mitigates the harmonics generated by the converter, ensuring a smooth AC output to the grid.
- Three phase inverter bridge: converts the stable DC voltage into a controlled AC output using the PWM technique.
- PLL: synchronizes the VSC with the grid.

- Inner Current Controller (ICC): generates the voltage references to be supplied to the PWM converter.
- Outer Power Controller (OPC): generates the current references to be supplied to the ICC during normal operation.
- Fault Current Injection (FCI): generates the current references to be supplied to the ICC during fault conditions.

A constant voltage source is considered because the goal of this thesis is to investigate the impact of fault current injection on AC side protections, excluding interactions between the DC and AC sides. Moreover, this assumption is considered valid because during a low-voltage situation, such as a fault, the converter current is strongly limited, typically between 1 and 1.2. As a result, the energy from the DC source cannot be fully delivered to the grid. Typically, the DC side incorporates a chopper circuit used to dissipate surplus energy during a fault, facilitating the assumption of a nearly constant DC-link voltage [22].

3.1.1 PI Controllers Tuning

The operation of the ICC, OPC, and PLL relies on PI controllers, hence correct tuning is essential.
The tuning of the PI controllers was carried out following the following approach: Firstly, the transfer functions of the individual elements comprising the specific block diagram were derived. Then, starting from the complete block diagram, the Simulink PID tuner tool was used for automatic parameter tuning.

It was crucial to consider the influence of terminal voltage on the tuning of the control systems, because during faults the voltage drops significantly. The ICC remains unaffected by voltage variations, ensuring stable current regulation. However, the PLL and the OPC are influenced by these changes. While the OPC is inactive during faults, the PLL may struggle with synchronization due to the reduced voltage. Thus, tuning must account for these conditions.

3.2 dq0 Reference Frame

The dq0 reference frame, or synchronous reference frame (SRF), is a coordinate system used in the analysis and control of three-phase electrical systems. It transforms three-phase quantities (like voltages and currents) into a rotating frame of reference rotating at θ^* angular speed. If θ^* is chosen as the system's angular frequency ($2\pi 50$), by transforming the system into the dq0 reference frame, the AC components, which would be sinusoidal in the stationary reference frame, become constant components.

Mathematically, this transformation is accomplished using the following equation:

$$\begin{bmatrix} d \\ q \\ 0 \end{bmatrix} = \frac{2}{3} \begin{bmatrix} \sin(\theta^*) & \sin(\theta^* - \frac{2\pi}{3}) & \sin(\theta^* + \frac{2\pi}{3}) \\ \cos(\theta^*) & \cos(\theta^* - \frac{2\pi}{3}) & \cos(\theta^* + \frac{2\pi}{3}) \\ \frac{1}{2} & \frac{1}{2} & \frac{1}{2} \end{bmatrix} \begin{bmatrix} a \\ b \\ c \end{bmatrix} \tag{1}$$

When this transformation is applied to a symmetric three-phase voltage:

$$v_{abc} = \begin{bmatrix} V \cdot \sin(\theta) \\ V \cdot \sin(\theta - \frac{2\pi}{3}) \\ V \cdot \sin(\theta + \frac{2\pi}{3}) \end{bmatrix} \tag{2}$$

The result in the dq0 reference frame is:

$$\begin{cases} v_d = \sqrt{\frac{3}{2}} \cdot V \cdot \cos(\theta - \theta^*) \\ v_q = \sqrt{\frac{3}{2}} \cdot V \cdot \sin(\theta - \theta^*) \end{cases} \tag{3}$$

If $\theta^* = \theta$:

$$\begin{cases} v_d = \sqrt{\frac{3}{2}} \cdot V \\ v_q = 0 \end{cases} \tag{4}$$

In this reference frame, the expression for active and reactive power are simplified to:

$$\begin{cases} P = \frac{3}{2}(v_d \cdot i_d + v_q \cdot i_q) \\ Q = \frac{3}{2}(v_q \cdot i_d - v_d \cdot i_q) \end{cases} \tag{5}$$

3.3 Grid Side Filter

The LCL filter is the filter topology chosen for this model (Figure 3), being the most commonly used filter in these applications. In the literature, many different design methodologies can be found. [15] proposes a simple and systematic design methodology, which will not be extensively discussed in this thesis.

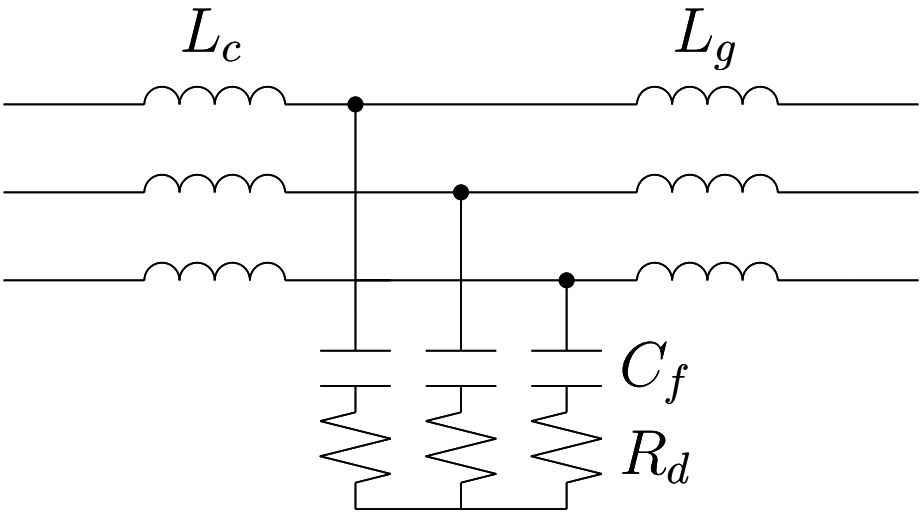

Figure 3: LCL filter with damping resistor

It is important to note that the resonance frequency of the filter must obey (6) in order to avoid resonance at low or high order frequencies. Additionally to further avoid the resonance problem, a damping resistor is added in series to the capacitor.

$$10 f_g \leq f_{res} \leq \frac{f_{sw}}{2} \tag{6}$$

f_g and f_{sw} are the grid and switching frequency respectively.

The resonance frequency of an LCL filter can be computed using:

$$f_{res} = \frac{1}{2\pi} \sqrt{\frac{L_c + L_g}{L_c \cdot L_g \cdot C_f}} \tag{7}$$

L_c and L_g are the converter side and grid side inductors.

To study the behaviour of the converter at the grid frequency (Essential for the ICC, Section 3.5) the influence of the capacitor C_f will be neglected since it only deals with the switching ripple frequencies. In fact, at frequencies lower than half of the resonance frequency the LCL filter and the L filter behave in

the same way. In other words the LCL filter based converter behaves as if the capacitor is not present, and the frequency characteristic of the LCL filter is equivalent to the frequency characteristic of a L filter made by the sum of the inductances downstream of the converter [24]:

$$L = L_c + L_g + L_s \tag{8}$$

L_s is the source inductance of the grid to which the filter is connected, if the grid is strong $L_s << L_c + L_g$ and therefore L_s could be omitted.

3.4 Synchronous Reference Frame Phase-Locked Loop (SRF-PLL)

A Phase-Locked Loop (PLL) is a control system that generates a signal with a phase that is synchronized to the phase of an input signal. In power systems, PLLs are essential for synchronization purposes, the input is the three phase grid voltage and the output is the phase angle (of one of the three phases). They ensure that converters, such as Voltage Source Converters (VSC), can properly align their output with the grid's voltage and frequency. This alignment is vital for the stability and efficiency of the power system, particularly in applications involving renewable energy sources and grid integration.

A Synchronous Reference Frame PLL (SRF-PLL) is a basic type of phase-locked loop based on the Park transform (Section 3.2), which simplifies the control and synchronization tasks. The phase angle θ is tracked by synchronizing the voltage space vector along the d-axis (in the dq reference frame), which in practice translates to zeroing the q component of the voltage.

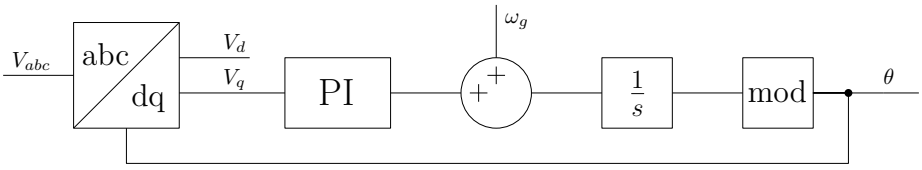

Figure 4: Block diagram of the SRF-PLL

Figure 4 illustrates the block diagram of the implemented SRF-PLL. The main components of the SRF-PLL include:

- Park Transformation (abc to dq0 Transformation):
  Converts the three-phase AC voltage (abc) into the direct-quadrature-zero (dq0) reference frame.
- PI Controller:
  Drives the q component of the voltage to zero.
- Integrator:
  Integrates the frequency to obtain the phase angle θ.
- Mod block:
  Wraps the phase angle θ between 0 and 2π.

Starting from the block diagram in Figure 4, the transfer functions of the SRF-PLL are derived.

The transfer function of the Park transformation can be derived from (4) by applying the small signal approximation:

$$V_q = \sqrt{\frac{3}{2}} \cdot V \cdot \sin(\theta - \theta^*) \approx \sqrt{\frac{3}{2}} \cdot V \cdot (\theta - \theta^*) \tag{9}$$

In (5) V is the line to line voltage across the converter's terminals. This approximation linearizes the system, allowing the derivation of the transfer function (10), and is based on the assumption that $\theta^* \approx \theta$ (which is the objective of the SRF-PLL).

$$G_{\mathrm{dq}}(s) = V \cdot \sqrt{\frac{2}{3}} \tag{10}$$

The transfer function of the other components of the PLL are straightforward:

$$G_{\mathrm{PI}}(s) = \frac{K_i + K_p s}{s} \tag{11}$$

$$G_I(s) = \frac{1}{s} \tag{12}$$

Knowing all the transfer functions, it is possible to derive the block diagram shown in Figure 5.

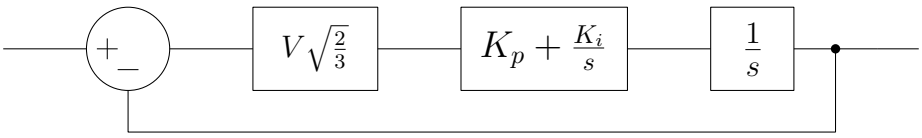

Figure 5: Small signal model of the SRF-PLL

Then the open loop transfer function of the SRF-PLL is:

$$G_{\mathrm{OL}}(s) = G_{\mathrm{dq}}(s) \cdot G_{\mathrm{PI}}(s) \cdot G_I(s) = V\sqrt{\frac{2}{3}} \cdot \frac{(K_i + K_p s)}{s} \cdot \frac{1}{s} \tag{13}$$

$$G_{\mathrm{OL}}(s) = V\sqrt{\frac{2}{3}} \cdot \frac{(K_i + K_p s)}{s^2} \tag{14}$$

(14) shows that the dynamic behaviour of the SRF-PLL is dependent on the voltage across the converter's terminals V: the lower the voltage the slower the response.

To meet the requirements of the fault current injection, reported in Section 2.1.1, the step response of the PLL during a fault must have a rise time of less than 30 ms and a settling time of less than 60 ms. This is a general condition that must be met even under the most severe fault conditions.
Therefore the tuned PI controller parameters must ensure not only proper dynamic behaviour but also adherence to these requirements.

In this thesis, the performance and dynamic behavior of the implemented PLL under fault conditions will not be evaluated; to delve deeper into these aspects, refer to [24] [22] [23] [14].

3.5 Inner Current Controller (ICC)

The purpose of the inner current controller (ICC) is to generate the voltage reference to be supplied to the PWM logic, in order to control active and reactive power exchange during normal operation, and to control the fault current injection during fault conditions.

To understand the control structure of the ICC, it is necessary to derive the operating equation of the system (VSC, filter and grid), i.e. the equation that describes the evolution of the grid current.
Figure 6a shows the VSC connected to the grid (represented with a RL impedance Z_s), defining v_c as the voltage across the converter and v_g as the grid voltage.

As explained in Section 3.3, it is possible to neglect the filter capacitor and the damping resistor without compromising the accuracy of the model at the grid frequency. Additionally, assuming a $\frac{X}{R}$ ratio of 10 for the grid impedance, the resistive component of the grid impedance can be neglected. Then the equation that describes the evolution of the grid current is (Figure 6b):

$$v_c = v_g + L\frac{di}{dt} \tag{15}$$

In (15) $L = L_c + L_g + L_s$ is the sum of the converter side inductor, the grid side inductor and the grid inductance.

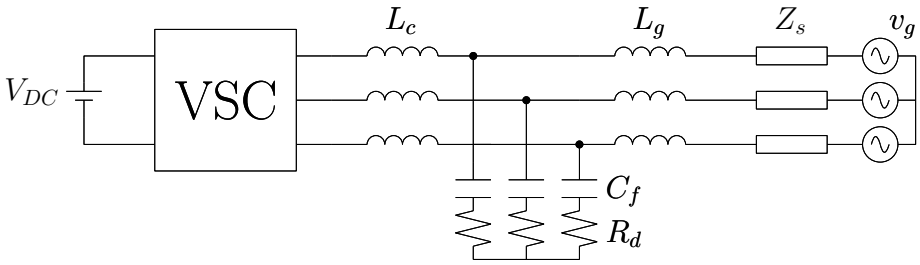

(a) VSC connected to the grid

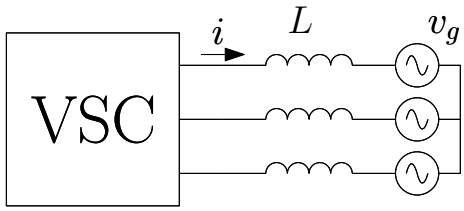

(b) Simplified network

Figure 6

Applying the Park transform to (15), the operating equation of the system is obtained in the dq reference frame:

$$\begin{cases} \dfrac{di_d}{dt} - \omega \cdot i_q = \dfrac{1}{L}(-v_{g_d} + v_{c_d}) \\ \dfrac{di_q}{dt} + \omega \cdot i_d = \dfrac{1}{L}(-v_{g_q} + v_{c_q}) \end{cases} \tag{16}$$

In the dq reference frame, the d and q differential equations for the current are dependent due to the cross coupling terms ωi_q and ωi_d (16).

Applying the Laplace transform to (16) the operating equations become:

$$\begin{cases} s \cdot i_d - \omega \cdot i_q = \dfrac{1}{L}(-v_{g_d} + v_{c_d}) \\ s \cdot i_q + \omega \cdot i_d = \dfrac{1}{L}(-v_{g_q} + v_{c_q}) \end{cases} \tag{17}$$

To achieve independent control of i_d and i_q it is necessary to compensate the cross coupling terms $\omega L i_q$ and $\omega L i_d$ and to feed forward the respective grid voltage dq component. Achieving independent control allows the use of two separate PI controllers, one for each axis, as shown in Figure 7.

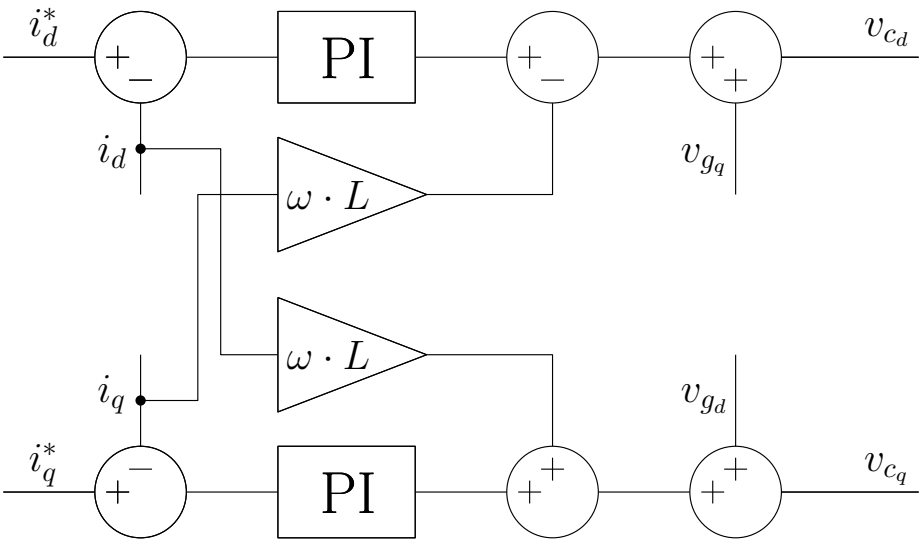

Figure 7: Block diagram of the ICC

With the compensation of the grid influence and of the cross coupling terms the controllers for both d and q axis currents can be designed on the basis of the filter transfer function [7]:

$$G_f(s) = \frac{1}{sL} \tag{18}$$

Figure 8 shows the block diagram of the feedback system.

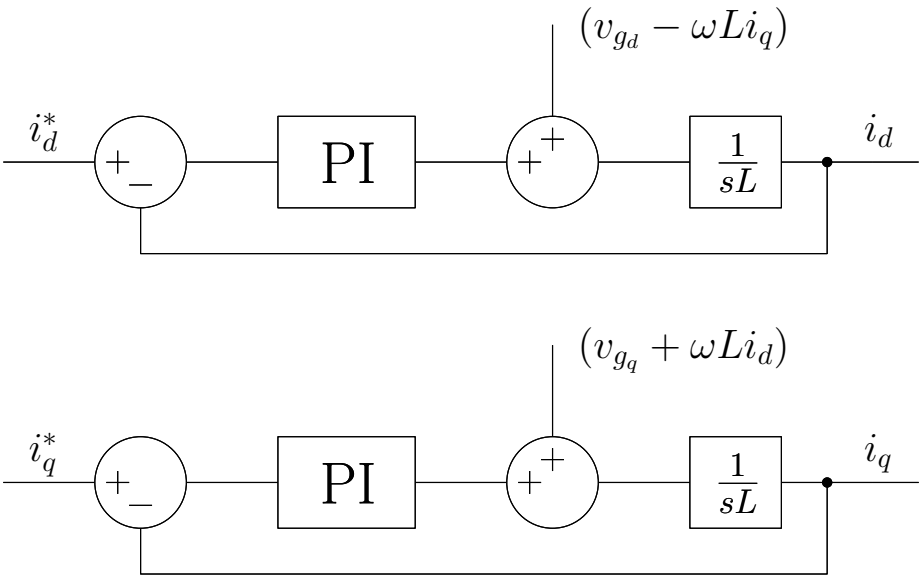

Figure 8: Block diagram of the ICC

Because the d and q axis are independent the two PI controllers can be tuned referring to the same reduced block diagram (Figure 9).

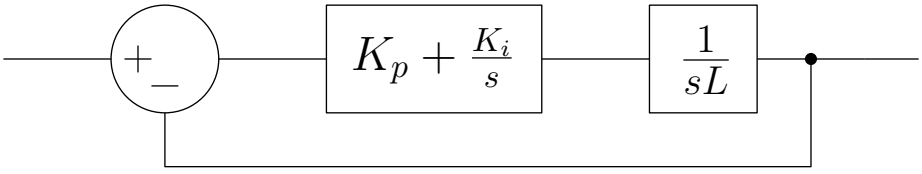

Figure 9: Reduced block diagram of the ICC

From Figure 9 the derivation of the open loop transfer function of the ICC is straightforward:

$$G_{\mathrm{OL}}(s) = G_{\mathrm{PI}}(s) \cdot G_f(s) = \frac{(K_i + K_p s)}{s} \cdot \frac{1}{sL} \tag{19}$$

$$G_{\mathrm{OL}}(s) = \frac{K_i + K_p s}{s^2 L} \tag{20}$$

(20) shows that the dynamic behaviour of the ICC is independent of the voltage across the converter's terminals; in fact, the only parameter affecting its

behaviour is the total inductance L.

To derive the transfer function of the OPC (Section 3.6), the closed-loop transfer function of the ICC is required:

$$G_{\mathrm{CL}}(s) = \frac{G_{\mathrm{OL}}(s)}{1 + G_{\mathrm{OL}}(s)} = \frac{\frac{K_i + K_p s}{s^2 L}}{1 + \frac{K_i + K_p s}{s^2 L}} \tag{21}$$

$$G_{\mathrm{CL}}(s) = \frac{K_i + K_p s}{s^2 L + K_i + K_p s} \tag{22}$$

3.6 Outer Power Controller (OPC)

The Outer Power Controller (OPC) is responsible for generating the current references, in the dq reference frame, to be supplied to the ICC during normal operation based on the desired values of active and reactive power.
The reference current d component is controlled to manage active power exchange while the reference current q component is controlled to manage the reactive power exchange. Sometimes the reference current d component is controlled also to perform the DC voltage regulation, this will not be the case in this thesis.

To understand the control structure of the OPC, it is necessary to consider the equations governing active and reactive power exchange in the dq reference frame (5):

$$\begin{cases} P = \dfrac{3}{2}(v_d \cdot i_d + v_q \cdot i_q) \\ Q = \dfrac{3}{2}(v_q \cdot i_d - v_d \cdot i_q) \end{cases} \tag{23}$$

Assuming that the d axis is perfectly aligned with the grid voltage $v_q = 0$ (this is the objective of the SRF-PLL, therefore as long as it is doing its job the assumption is valid), the active power and the reactive power will therefore be proportional to i_d and i_q respectively:

$$\begin{cases} P = \dfrac{3}{2} v_d \cdot i_d \\ Q = -\dfrac{3}{2} v_d \cdot i_q \end{cases} \tag{24}$$

The voltage and current components in the synchronous dq frame must be properly filtered before they can be manipulated in the previous active and reactive power formulas, because the objective of the OPC is to regualate the first harmonic active and reactive power exchange [24]. A second-order low-pass filter was used for filtering.
Figure 10 shows the block digram of the OPC. Figure 11 shows the block diagram of the feedback system.

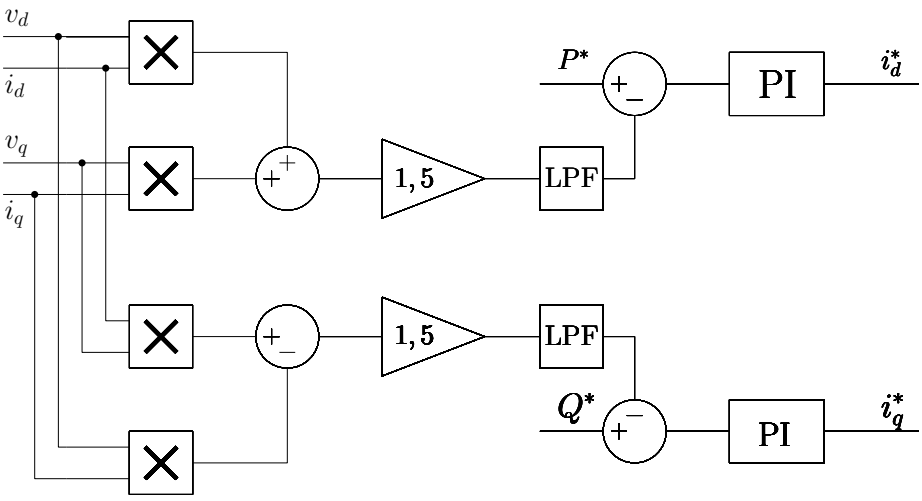

Figure 10: Block diagram of the OPC

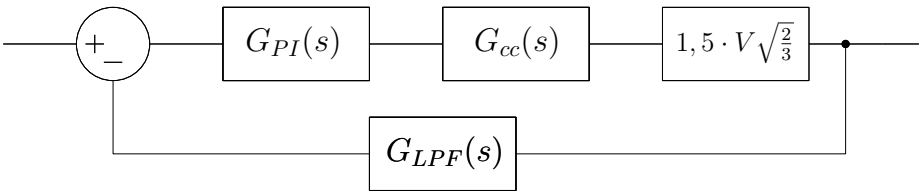

Figure 11: Block diagram of the feedback system (Active power)

The transfer functions of the blocks shown in Figure 11 are provided below. From these, the derivation of the open-loop transfer function of the OPC is straightforward.
It is important to note that in Figure 11 and in the subsequent equations, reference is made to the loop that controls active power, as the term $1,5 \cdot V\sqrt{\frac{2}{3}}$ is used to evaluate P. To determine the open loop transfer function for the reactive power loop, it is sufficient to add a minus sign to the subsequent equations ($-1,5 \cdot V\sqrt{\frac{2}{3}}$ as in (24)).

G_{cc} is the closed-loop transfer function of the ICC (Equation 22), the term $1,5 \cdot V\sqrt{\frac{2}{3}}$, where V is the line to line voltage, derives from (24).

$$G_{\mathrm{LPF}}(s) = \frac{\omega_n^2}{s^2 + 2\zeta\omega_n s + \omega_n^2} \tag{25}$$

$$G(s) = G_{\mathrm{PI}}(s) \cdot G_{\mathrm{cc}}(s) \cdot 1,5 \cdot V\sqrt{\frac{2}{3}} \tag{26}$$

$$G(s) = \frac{(K_{i_{pc}} + K_{p_{pc}} s)}{s} \cdot \frac{(K_{i_{cc}} + K_{p_{cc}} s)}{(s^2 L + K_{i_{cc}} + K_{p_{cc}} s)} \cdot 1,5 \cdot V \sqrt{\frac{2}{3}} \tag{27}$$

$$G_{\mathrm{OL}}(s) = G(s) \cdot G_{\mathrm{LPF}}(s) \tag{28}$$

$$G_{\mathrm{OL}}(s) = \frac{(K_{i_{pc}} + K_{p_{pc}} s)}{s} \cdot \frac{(K_{i_{cc}} + K_{p_{cc}} s)}{(s^2 L + K_{i_{cc}} + K_{p_{cc}} s)} \cdot 1,5 \cdot V \sqrt{\frac{2}{3}} \cdot \frac{\omega_n^2}{(s^2 + 2\zeta\omega_n s + \omega_n^2)} \tag{29}$$

(29) shows that the dynamic behaviour of the OPC is dependent on the voltage across the converter's terminals V, therefore, during a fault, the dynamics of the OPC are affected by the voltage variation; however, this is not an issue since, during fault conditions, the OPC is excluded from the control loop because the FCI block (Section 3.7) takes over, generating current references during fault conditions. Thus, in summary, the tuning of the PI controllers is performed considering only nominal operating conditions.

When tuning the PI controllers of the OPC, it is very important to obtain a step response much slower than the one of the ICC to ensure the decoupling of the two control systems.

3.7 Fault Current Injection Block

The fault current injection block is responsible for generating the current references to be supplied to the ICC during fault conditions. The determination of the current reference is based on the guidelines provided in the considered grid code; in this thesis, reference is made to the German grid code (Section 2.1.1), whose requirements are summarized in Table 1.

The current supplied by the converter must be less than the maximum current I_{max}; therefore, the following condition must hold:

$$\sqrt{i_d^2 + i_q^2} < I_{max} \tag{30}$$

During a fault, the converters must supply as much current as possible; therefore, if the reactive component (to which is given priority) does not reach the maximum deliverable current, the residual current is supplied by the active component according to:

$$i_d = \sqrt{I_{max}^2 - i_q^2} \tag{31}$$

Figure 12 shows the block diagram of the fault current injection block, which activates only if the voltage drops below 10 % of the nominal line to line voltage V_n (Table 1).

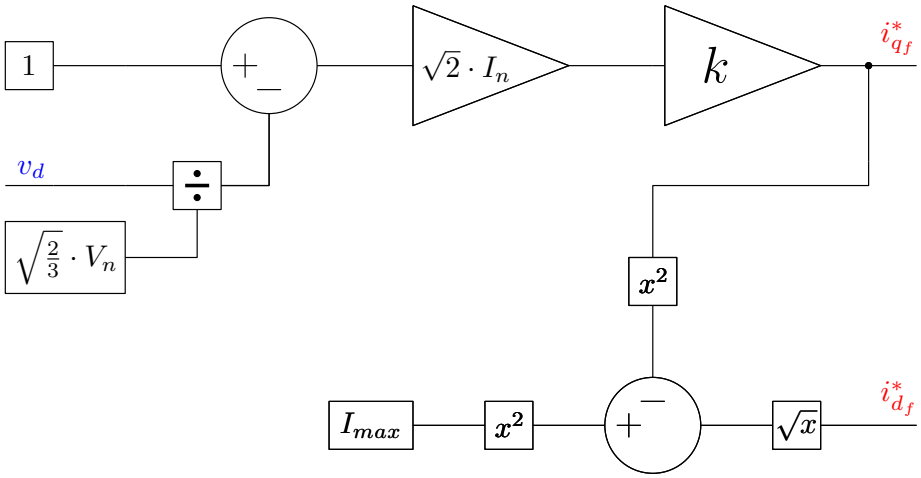

Figure 12: Block diagram of the FCI block

3.8 Simulation results

This section describes the different simulations of the VSC converter carried out in Matlab-Simulink®. The parameters and references used in each simulation are presented. First, the operation of the VSC converter under normal operating conditions is simulated, with varying active and reactive power references over time. Subsequently, the operation under fault conditions with different residual voltage values is simulated. The simulated faults will be bolted three-phase faults (Section 1.2).

The grid connected VSC is shown in Figure 13.

In Table 2 all the system's parameters used during the simulations are presented. The filter parameters are reported in Table 3 and the tuned PI controllers parameters are reported in Table 4.

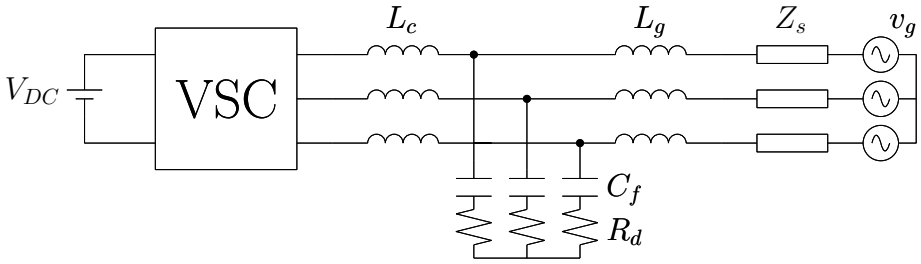

Figure 13: Grid connected VSC used in the simulations

Parameter	Description	Value
V_{LL}	Line to line RMS grid voltage	400 V
S_n	Rated power	100 kVA
f_g	Grid frequency	50 Hz
f_{sw}	Switching frequency	10 kHz
I_n	Rated current	144,34 A
I_{max}	Maxiumum current (peak value)	224,54 A
V_{DC}	DC Voltage	800 V
k	Fault current injection k factor	2
Grid		
S_{sc}	Short circuit power	100 MVA
$\frac{X}{R}$	$\frac{X}{R}$ ratio	10

Table 2: System parameters

The Maximum current reported in Table 2 is calculated assuming an increase of 10 % above the rated current: $I_{max} = 1,1 \cdot I_n \cdot \sqrt{2}$.

Parameter	Description	Value
C_f	Filter capacitor	100 μF
L_c	Converter side inductor	0,5 mH
L_g	Grid side inductor	0,15 mH
R_d	Damping resistor	3,58 Ω
f_{res}	Filter resonance frequency	1482 Hz

Table 3: LCL filter parameters

Parameter	Description	Value
$K_{p_{PLL}}$	PLL Proportional gain	10
$K_{i_{PLL}}$	PLL Integral gain	10000
$K_{p_{cc}}$	ICC Proportional gain	10
$K_{i_{cc}}$	ICC Integral gain	10000
$K_{p_{pc}}$	OPC Proportional gain	0
$K_{i_{pc}}$	OPC Integral gain	0,2

Table 4: PI controllers tuned parameters

3.8.1 Normal operating conditions

This section presents the results of the simulation conducted under normal operating conditions, in which time varying active and reactive power references where assigned. In Table 5 the order of events during the simulations is presented.
At the beginning of the simulation, the converter is required to supply half of its nominal power, 0,5 pu, with a power factor of 1 ($cos\varphi = 1$). At t = 0,2, the power reference doubles, maintaining the power factor unchanged, reaching the nominal power of 1 pu. At t = 0,4, the active power reference decreases to 0,8 pu, and the converter is required to supply 0,6 pu of reactive power, operating with a power factor of 0,8. Finally, at t = 0,6, maintaining the power factor unchanged, the converter supplies reactive power of the opposite sign.

Time instant [s]	Active power reference [pu]	Reactive power reference [pu]
0	0,5	0
0,2	1	0
0,4	0,8	- 0,6
0,6	0,8	0,6

Table 5: Simulation order of events

In Figure 14 the results of the simulation are presented, showing the time

evolution of the main quantities involved. The results indicate the correct operation of the converter, which is able to track the assigned active and reactive power references.

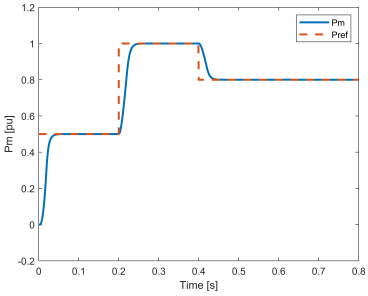

(a) Active power reference Pref and Active power measurement Pm

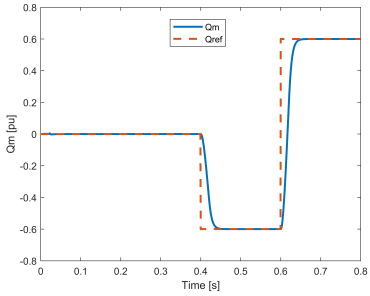

(b) Reactive power reference Qref and Reactive power measurement Qm

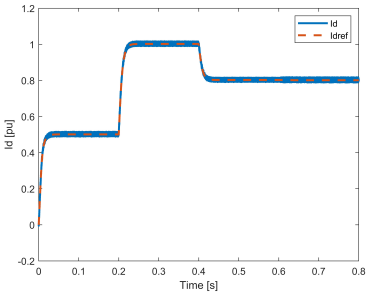

(c) Active current reference Idref and Active current measurement Id

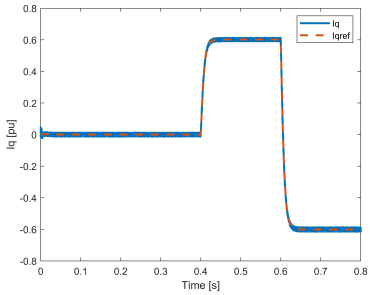

(d) Reactive current reference Iqref and Reactive current measurement Iq

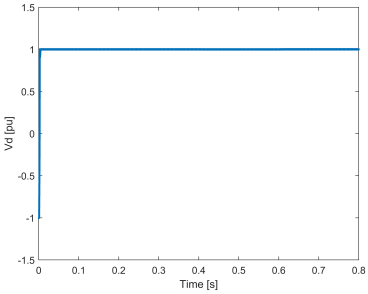

(e) Voltage d component Vd

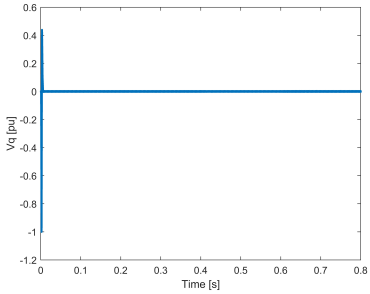

(f) Voltage q component Vq

Figure 14: VSC simulation results during normal operation

3.8.2 Fault Behaviour

This section presents the results of the simulation conducted under fault conditions.

In Table 7 the order of events used during the simulations is presented. At the beginning of the simulation, the converter ramps up to nominal power 1 pu, with a power factor of 1 ($cos\varphi = 1$). Subsequently, three three-phase bolted faults are applied, at the converters terminals, in succession with three different residual voltages, i.e. three different voltage drops.

Time instant [s]	Description
0	Normal operation: Pref = 1 pu Qref = 0 pu
0,1	Fault with residual voltage of 0,85 pu
0,16	Fault with residual voltage of 0,51 pu
0,22	Fault with residual voltage of 0,06 pu

Table 6: Simulation order of events

In Figure 15 and Figure 16 the results of the simulation are presented, showing the time evolution of the main quantities involved. The results indicate the correct operation of the converter, which is able to track the assigned reactive and active current references during the faults.

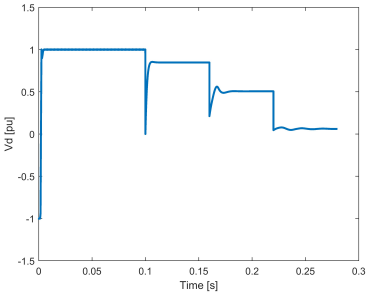

(a) Voltage d component Vd

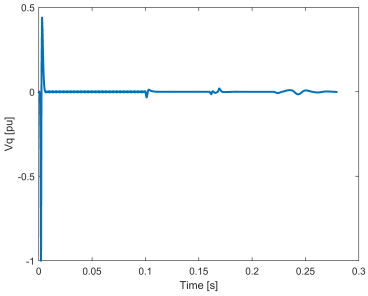

(b) Voltage q component Vq

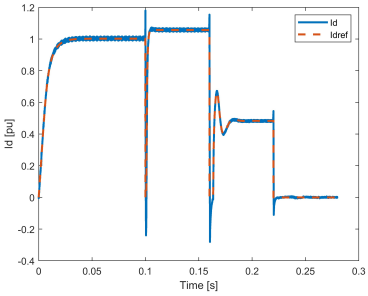

(c) Active current reference Idref and Active current measurement Id

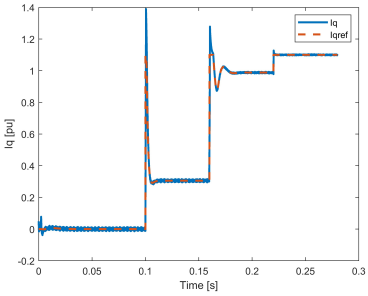

(d) Reactive current reference Iqref and Reactive current measurement Iq

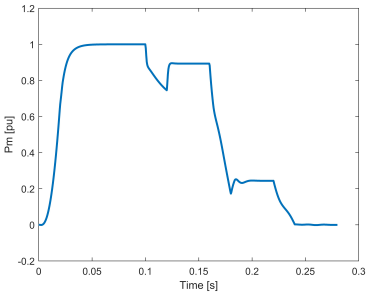

(e) Active power measurement Pm

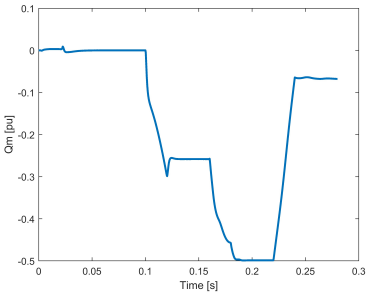

(f) Reactive power measurement Qm

Figure 15: VSC simulation results during fault conditions

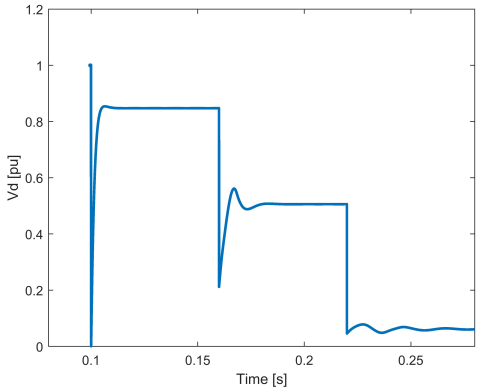

(a) Voltage d component Vd

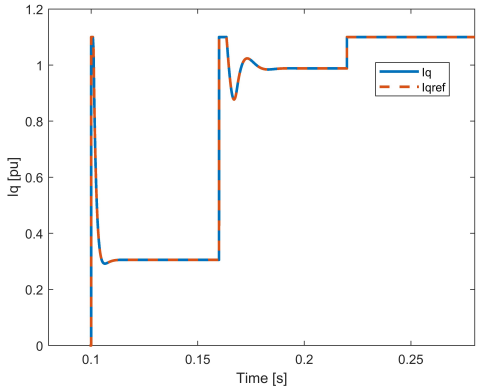

(b) Active current reference Idref and Active current measurement Id

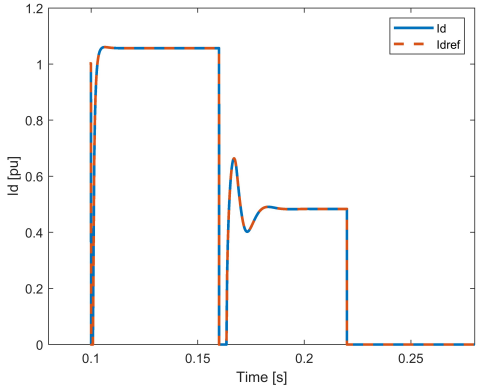

(c) Reactive current reference Iqref and Reactive current measurement Iq

Figure 16: VSC simulation results during fault conditions close up

Verification of the operation of the fault current injection block

To verify the correct operation of the fault current injection block (Section 3.7), the reactive and active current references to be provided to the ICC will be manually calculated based on the guidelines of Table 1 and equations (31) and (30).
This block is responsible for the correct application of the guidelines related to fast fault current injection as outlined in the grid code (in this thesis, the German grid code), therefore it is important to verify its operation. Table 7 reports the performed calculation.

Residual voltage (Voltage drop) [pu]	Reactive current reference [pu]	Active current reference [pu]
0,85 (0,15)	$i_q = k \cdot \Delta v = 2 \cdot 0,15 = 0,3$	$i_d = \sqrt{i_{max}^2 - i_q^2} = \sqrt{1,1^2 - 0,3^2} = 1,06$
0,51 (0,49)	$i_q = 2 \cdot 0,49 = 0,98$	$i_d = \sqrt{1,1^2 - 0,98^2} = 0,5$
0,06 (0,94)	$i_q = 2 \cdot 0,94 = 1,96 \rightarrow i_q = 1,1$	$i_d = 0$

Table 7: Active and reactive current references calculation

The values obtained in Table 7 are consistent with those shown in Figure 16, confirming the correct operation of the converter under fault conditions.

4 IQ Distance Protection: the TD21 Element

4.1 Introduction

Incremental Quantities (IQ) line protections are a type of time domain protections that were first introduced in [9] to determine fault direction. Protection elements implementing this principle can reliably operate in milliseconds [19] for this reason they are often referred to as ultra high speed protections.

In this section, the incremental quantities distance protection element TD21, incorporated in the SEL-T400L relay, produced by Schweitzer Engineering Laboratories (SEL), will be implemented using the articles written by SEL itself [19] [17] [16] [12] and the instruction manual [5] as references. The TD21 distance element provides instantaneous underreaching line protection. Therefore it can be used for tripping directly without communications.

The chapter is divided as follows: in Section 4.2 the concept of Incremental Quantities is presented; in Section 4.3 and 4.4 the operation and logic behind the TD21 element are described; in Section 4.5 the testing criteria adopted to validate the element are discussed; in Section 4.6 the results of the performed simulations are presented; in Section 4.7 the application to unbalanced faults is briefly discussed.

4.2 Incremental Quantities (IQ)

Incremental quantities, often referred to as superimposed quantities, are incremental changes between the present values of a signal (in the context of electric systems, currents and voltages) and their n cycles old values, typically one or two cycles old.

$$\Delta s(t) = s(t) - s(t - nT) \tag{32}$$

Where T is the signal period.
They are fault-induced components because under normal operation, they are null. For this reason, they are implemented in protection systems.

Consider two network terminals connected by a transmission line, and assume that a three phase symmetric fault occurred at a distance m in per-unit value from the left bus (Figure 17), to solve the faulted network, we can apply the superposition principle [20], as shown in Figure 18.

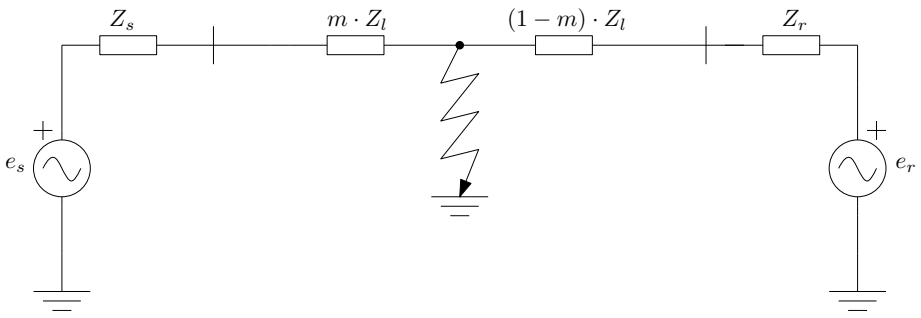

Figure 17: Fault in a two terminal network (Single-phase equivalent circuit)

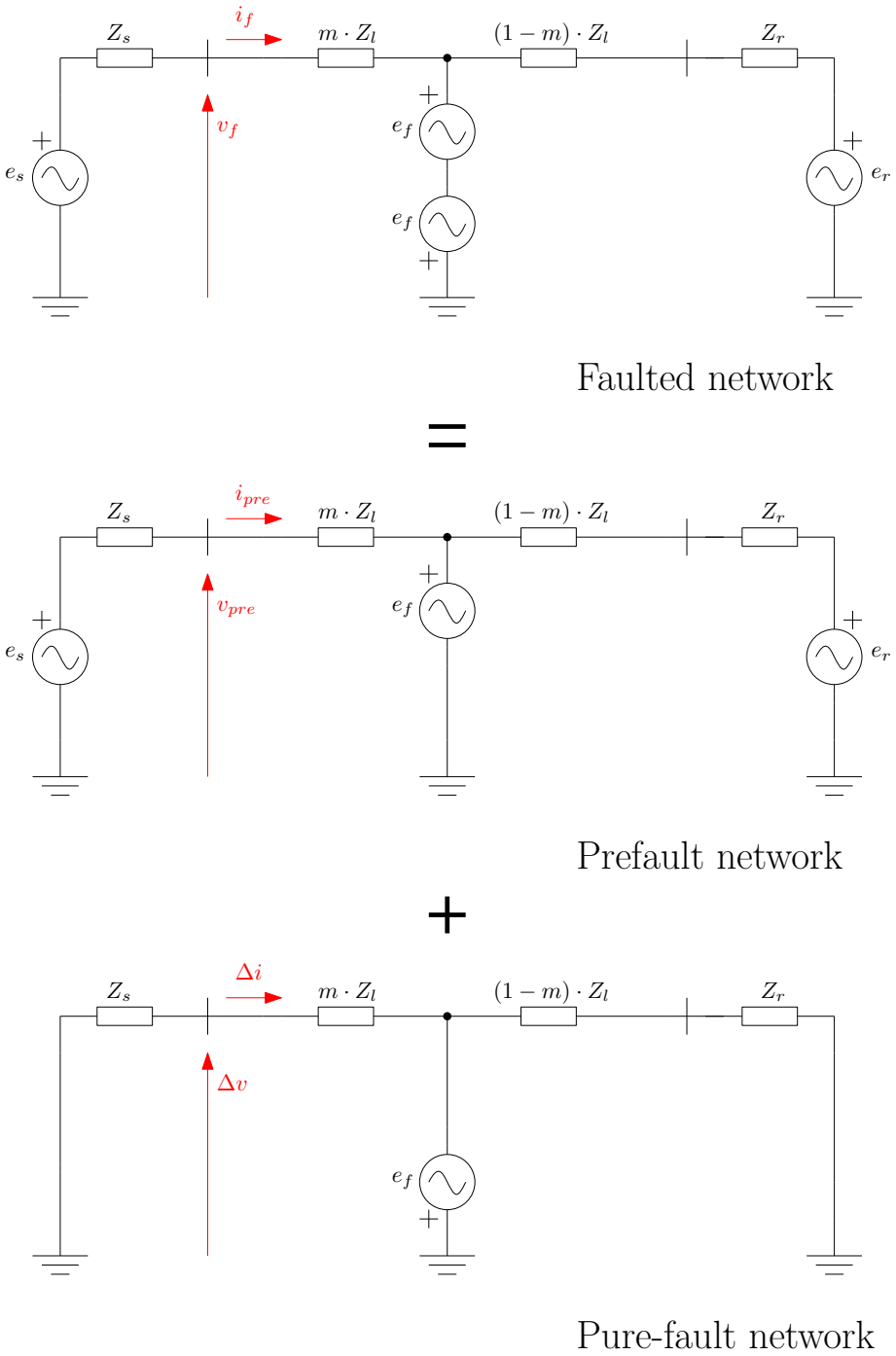

Figure 18: Superposition principle applied to a faulted network

In the faulted network, the fault branch is represented by two series voltage sources with a magnitude equal to the pre-fault voltage (e_f) present at the fault point. Because the two generators produce equal but opposite voltages, their series is equivalent to a short circuit.
In the pre-fault network, the voltage source can be removed because it has no effect. The voltages and currents in the faulted circuit are equal to the sum of the voltages and currents in the pre-fault circuit and the voltages and currents in the pure-fault circuit:

$$i_f = i_{pre} + \Delta i \tag{33}$$

$$v_f = v_{pre} + \Delta v \tag{34}$$

Rearranging:

$$\Delta i = i_f - i_{pre} \tag{35}$$

$$\Delta v = v_f - v_{pre} \tag{36}$$

The only effect of the power system sources (e_s and e_r) and load flow, on Δv and Δi, is establishing the initial conditions for the superposition source e_f, other than that they depend only on the network parameters (Z_s, Z_r and Z_l) and on the fault location m.

The pre-fault values are n cycles old compared to the fault values, therefore using 36 and 35, we obtain incremental quantities that lasts for n power cycles, after which they expire because the historical values, i.e. the pre-fault values, we subtract slide into the fault period.

4.3 TD21 Principle of Operation

The TD21 distance element calculates, in time domain, the change in the voltage at the set reach point m_0 by using the measured currents and voltages at the relay location and the line resistance and inductance parameters [5] (Figure 19a). The element should reach up to the reach point m_0 on the protected line short of the remote bus and should not respond to faults beyond that point.

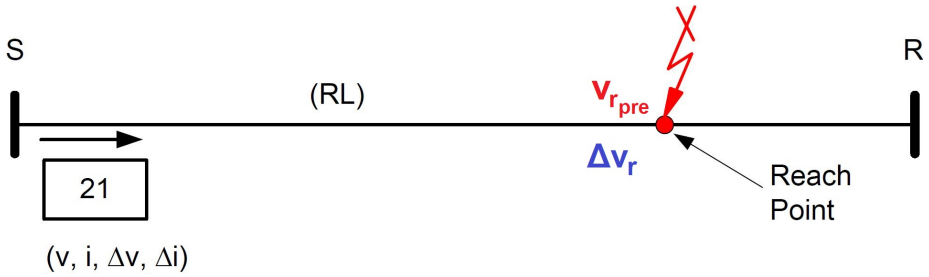

(a) Input data and measurements for the TD21 distance element

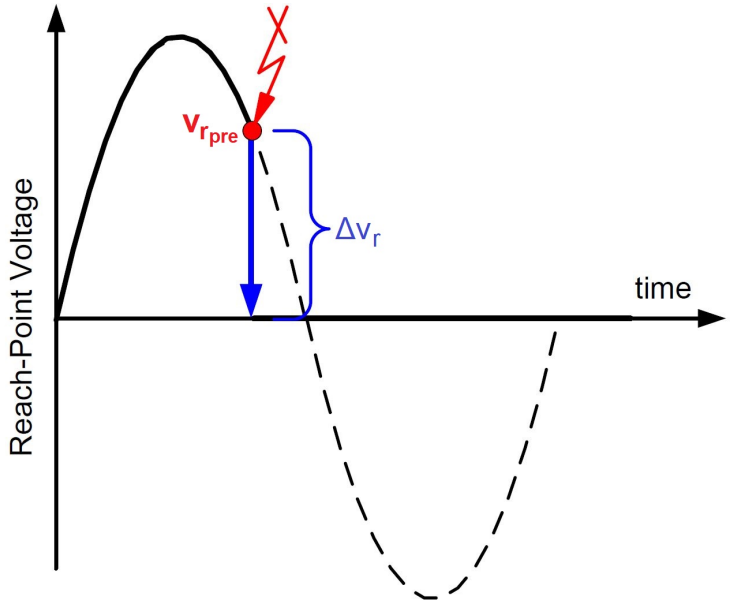

(b) Voltage at the reach point for a bolted fault at the reach point

Figure 19: Bolted fault at the reach point [18]

The TD21 principle of operation is based on the following observation: a bolted fault located exactly at the reach point causes a change in voltage at the reach point (Δv_r) equal to $-v_{r_{pre}}$ (Figure 19).

$$\Delta v_r = v_{r_f} - v_{r_{pre}} \tag{37}$$

During a bolted fault $v_{r_f} = 0$.

$$\Delta v_r = 0 - v_{r_{pre}} = -v_{r_{pre}} \tag{38}$$

Therefore the highest physically possible change in voltage at the reach point is the pre-fault voltage at the reach point [18].

Now consider a fault located short of the reach point as in Figure 20a. If you calculated the change in voltage at the reach point for this fault, you would obtain a value higher than the pre-fault voltage at the reach point. Consider now a fault located beyond the reach point as in Figure 20b. If you calculated the change in voltage at the reach point for this fault, you would obtain a value lower than the pre-fault voltage at the reach point [18].

Therefore, if the change in voltage at the reach point is greater than the pre-fault voltage, the element must intervene. This translates into the following operating equation:

$$|\Delta v_r| > \left|v_{r_{pre}}\right| \tag{39}$$

If this condition is true the fault is inside the protected zone and the element must intervene.

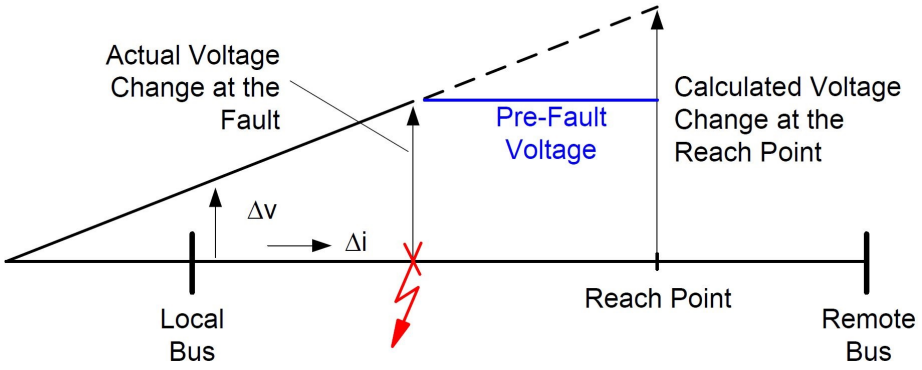

(a) In-zone fault

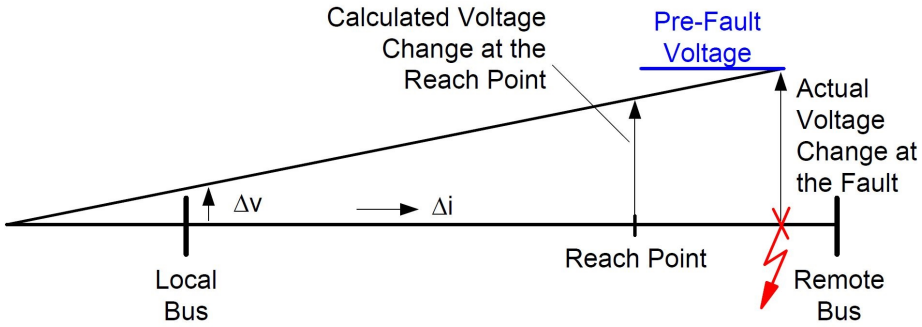

(b) Voltage at the reach point for a bolted fault at the reach point

Figure 20: Actual change in voltage at the fault location and change in voltage at the reach point that the distance element calculates [18]

4.3.1 Evaluation of the reach point voltage

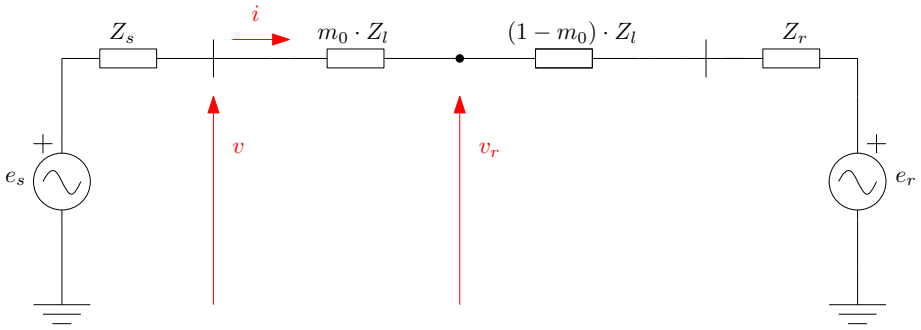

Figure 21: Voltage at the reach point in a two terminal network (Single-phase equivalent circuit)

The element must evaluate the voltage at the reach point in order to work. To do this, the protected line is represented as a series of an inductance and a resistance (Figure 21). Then the following equations can be written for the voltage v_r at the set reach point m_0:

$$v_r = v - m_0 \cdot \left(R_l \cdot i + L_l \cdot \frac{di}{dt} \right) \tag{40}$$

$$v_r = v - m_0 \cdot \left(R_l \cdot i + L_l \cdot \frac{di}{dt} \right) \cdot \frac{Z_l}{Z_l} \tag{41}$$

$$v_r = v - m_0 \cdot \left(\frac{R_l}{Z_l} \cdot i + \frac{L_l}{Z_l} \cdot \frac{di}{dt} \right) \cdot Z_l \tag{42}$$

Often, when incremental quantities are used, the expression "replica current" i_z is introduced, which essentially corresponds to a voltage drop. In this case, it helps simplify the equations governing the operation of the distance protection element.

$$i_z = \frac{R_l}{Z_l} \cdot i + \frac{L_l}{Z_l} \cdot \frac{di}{dt} \tag{43}$$

Then Equation 42 can be simplified as:

$$v_r = v - m_0 \cdot i_z \cdot Z_l \tag{44}$$

4.4 TD21 logic

In this chapter the implemented model will be described. Figure 22 shows the operating logic of the element: starting from the voltage and current measurements at the relay terminals to the determination of the fault presence within the protected line section (Output signal).

In the implementation of the element, some simplifications have been adopted:

- The logic capable of identifying the beginning of the fault has not been implemented.
- The element is capable of operating only on symmetrical three-phase faults, since these are the only faults that will be analysed in this thesis, in Section 4.7 the application to unbalanced faults will be briefly discussed.

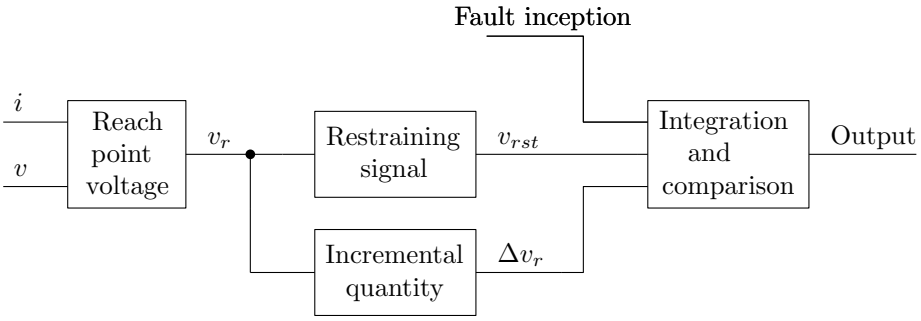

Figure 22: Block diagram of the implemented TD21 element

The *Reach point voltage* block implements Equations 44 and 43 to evaluate v_r, the *Incremental quantity* block applies the definition of IQ, by subtracting the n cycle old value of v_r to its present value, to obtain Δv_r.

The *Restraining signal* and *Integration and comparison* blocks will be described in the following sections.

4.4.1 Restraining signal

The TD21 element does not directly apply the operating equation 39: instead of using $\left|v_{r_{pre}}\right|$ directly as a restrictive signal, it applies modifications to the latter. This is necessary because in a real transmission line, the reach point voltage calculated with Equation 44 provides an approximation of the actual voltage because it is determined by considering the line as an RL element. Therefore, to make the element safer and more reliable, it is necessary to use a more complex restrictive signal v_{rst}.

Figure 23a explains the calculation of the restraining signal v_{rst}. The absolute value of the voltage at the reach point v_r is multiplied by the factor k

(slightly above 1) to add a small amplitude margin. To add a small phase margin n cycle old data (the delayed value of v_r is needed to represent the voltage at the reach point prior to the fault $v_{r_{pre}}$) and two extra sets of data, one ahead (*forward*) and one beyond (*backward*) the exact n cycle old data, are extracted. The two extra sets of data are used to create a security band (SB) around $v_{r_{pre}}$ (See Figure 23b).

The maximum value among the minimum restraint level and these three values becomes the final restraining signal v_{rst}. The minimum restraining level is a percentage of the peak value of v_r (increased by k), in fact MRL is a constant between 0 and 1. The minimum restraint level is used to ensure that the restraining signal v_{rst} does not fall to zero near the zero crossings.

The objective of this procedure is to create a signal that envelops the actual reach point voltage while assuming various sources of errors (for example instrument transformer errors and relay measurement errors), yet is as small as possible to maintain the speed and sensitivity inherent in the time-domain implementation [18]. Figure 23b shows an example of this procedure.

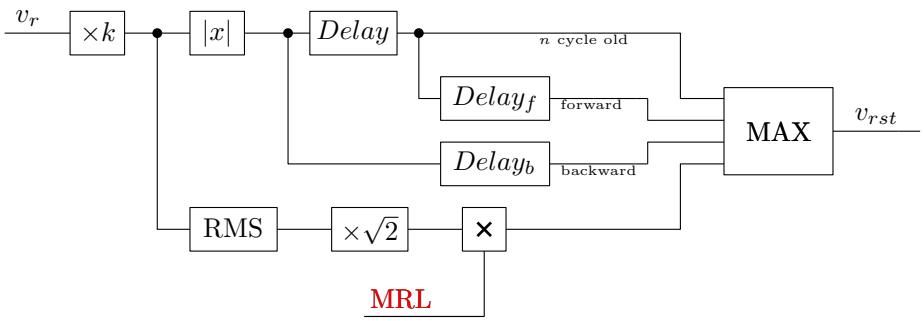

(a) Block diagram of the TD21 restraining signal

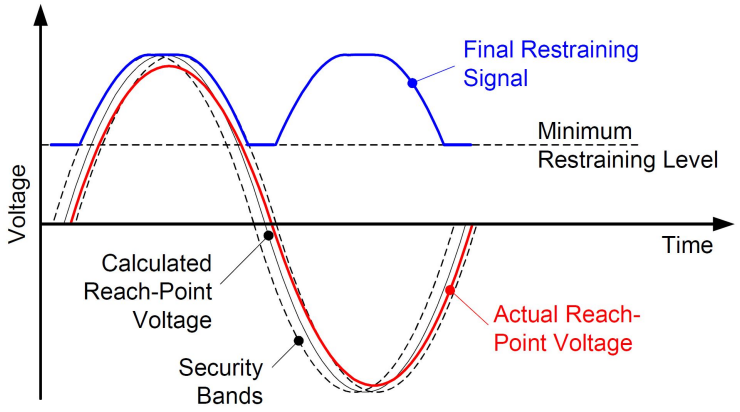

(b) Example of operation of the TD21 restraining signal [18]

Figure 23

4.4.2 Integration and comparison

The operating signal $|\Delta v_r|$ and the restraining signal v_{rst} are compared as shown in Figure 24a.
To add an extra layer of security the TD21 element asserts the presence of a fault only if the integral of the difference between the operating signal and the restraining signal is greater than a certain threshold, the security margin (SM):

$$\int (|\Delta v_r| - v_{rst})dt > SM \tag{45}$$

The integrator is run, by the enable signal (EN in Figure 24a), only if two conditions are met:

- The operating signal is greater than the restraining signal $|\Delta v_r| > v_{rst}$
- The fault identification logic (*Fault inception* in Figure 24a) confirms the presence of the fault (not implemented in this thesis).

Figure 24b shows an example of how the logic works.

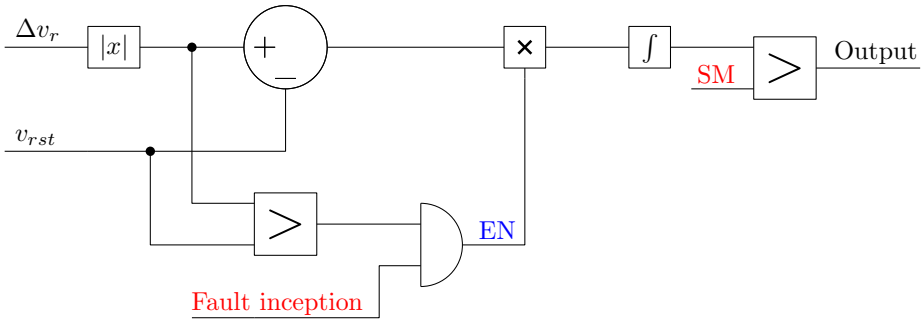

(a) Integration and comparison block diagram

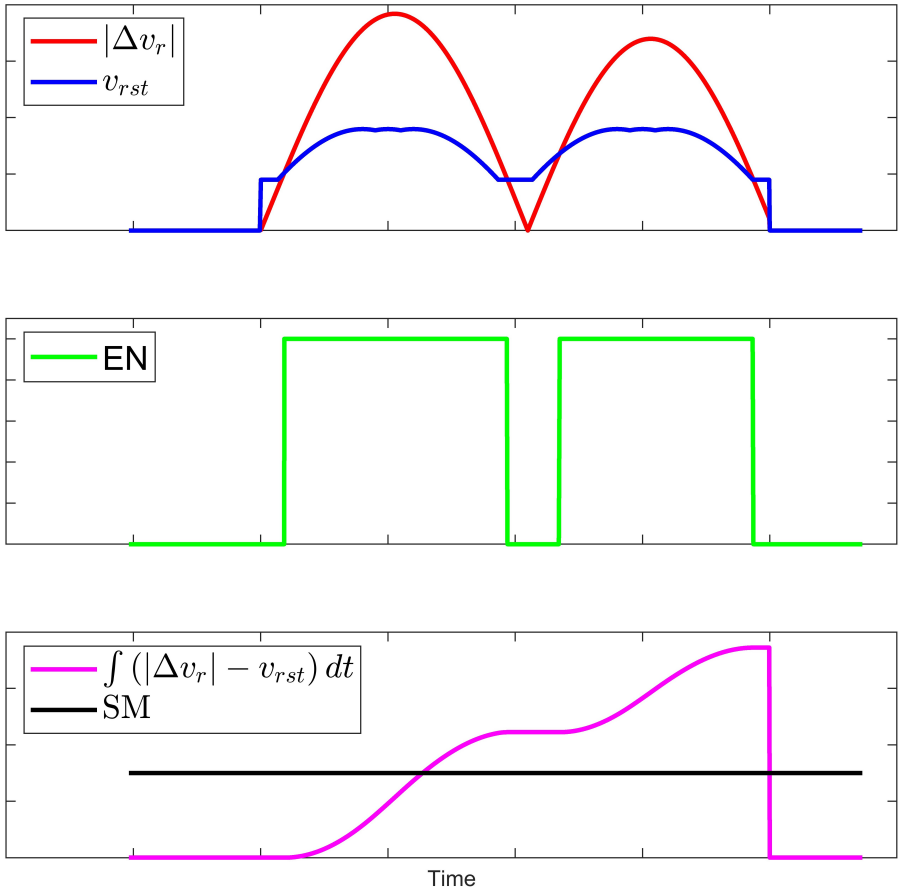

(b) Example of operation of the integration and comparison logic: the integration is performed only if the EN signal is high

Figure 24

4.4.3 Effect of settings on operation

In this section, the effect of the operational parameters (settings) of the TD21 element on its performance will be discussed.
The signals that determine the performance of the element are the restraining signal v_{rst} and the security margin (SM).

The restraining signal is determined by the following parameters (Section 4.4.1):

- Security factor (k)
- Security band (SB)
- MRL

As described in Section 4.4.1 the Security factor adds an amplitude margin and the Security band adds a phase margin, and together with the MRL they create a signal that envelopes the pre-fault reach point voltage. In fact $v_{rst} = \left|v_{r_{pre}}\right|$ if:

- $k = 1$
- $SB = 0$
- $MRL = 0$

The more the restraining signal resembles the pre-fault voltage at the reach point, the faster the protection element will respond, but the less secure it will be, as it will be more susceptible to errors. Causes of error include: evaluation of the reach point voltage by modelling the line with an RL impedance; measurement errors; voltage drop not caused by faults. The same reasoning applies to the SM, the lower it is the faster the protection element will respond, but the less secure it will be.

4.5 Testing criteria

To test a protection element, it is necessary to define criteria to evaluate its performance.

There are various criteria for testing the performance of a protection element [17]. The most relevant ones for the purpose of this thesis, and consequently those that will be used for evaluation, are the following:

- *Speed*, the time between fault inception and a trip command to the circuit breakers.
- *Dependability*, the ability to trip line faults under assumed operating and fault conditions.
  In the literature dependability is not defined rigorously [17]. In this thesis, dependability will be measured as a percentage of total in zone faults for which the element operates.
- *Security*, the ability to restrain for all conditions other than line faults, especially for out-of-zone faults

Speed, Dependability and Security of a protection element are influenced by several factors:

- Fault location along the line: The closer the fault is to the reach, the more the distance element struggles to detect its presence.
- Fault point on wave, i.e. the temporal point within the AC voltage cycle at which the fault is introduced: The protection algorithm needs to be effective regardless of the fault occurrence time within the voltage cycle.
- Source impedance ratio (SIR), analysed in Section 4.5.1.
- Fault resistance
- Fault type

In this thesis, only three phase bolted faults will be considered, therefore fault resistance and fault type will not be considered as parameters for performance analysis.

The *Speed* of the incremental quantities based elements is primarily determined by how rapidly the required incremental quantities develop. This is primarily a function of the impedance between the source and the fault point, and the voltage change at the fault point [17]. The latter depends on the pre-fault voltage at the fault point (point on wave).

The main criteria that challenge the *Dependability* of the incremental quantities based elements is whether the fault generates high enough incremental

voltage and current quantities given the minimum pickup thresholds [17].

With the results obtained from the simulations, the intervention time curve and the dependability curve will be plotted. The intervention time curve shows the intervention time as a function of the fault location. The dependability curve illustrates the percentage of faults that the element was able to detect based on the fault location, thereby also containing information on security, as it will indicate whether or not the element intervened for faults occurring outside the protected zone.

4.5.1 Source impedance ratio (SIR)

The SIR is the ratio of the source impedance (short circuit impedance) to the line impedance:

$$SIR = \frac{Z_s}{Z_l} \tag{46}$$

The SIR is well established as the preferred method for classifying the electrical length of a line for the purpose of applying protective relays [25]. IEEE C37.113, IEEE Guide for Protective Relay Applications to Transmission Lines [3] classifies line length based on SIR as follows:

- Long line (SIR $<$ 0,5)
- Medium line (0,5 $<$ SIR $<$ 4)
- Short line (SIR $>$ 4)

The SIR provides information about the three-phase short circuit power S_{sc} (and consequently about the three-phase short circuit current I_{sc}):

$$Z_s = \frac{V^2}{S_{sc}} \tag{47}$$

$$SIR = \frac{V^2}{S_{sc} \cdot Z_l} \tag{48}$$

$$SIR = \frac{V^2}{\sqrt{3} \cdot V \cdot I_{sc} \cdot Z_l} \tag{49}$$

$$SIR = \frac{V}{\sqrt{3} \cdot I_{sc} \cdot Z_l} \tag{50}$$

The higher the SIR (the shorter the line), the lower the short-circuit current contribution from the grid. This relationship is significant because a high SIR can influence the fault detection capability of protective devices. As the line gets shorter, the impedance decreases, leading to a reduced fault current contribution from the grid.

4.6 Simulation: TD21 testing and validation

In this section the implemented TD21 model will be tested and validated using the criteria defined in the previous chapters.

To test the developed protection model, a series of simulations in Matlab-Simulink® involving three-phase bolted faults on a medium voltage transmission line have been conducted, Table 8 lists the bus and line characteristics. The simulations are designed to evaluate the algorithm's performance under variable conditions.

Rated line to line voltage	20 kV
Nearby bus SCP [SIR]	100 MVA [2,4]
Remote bus SCP	variable
Line resistance	0,1 Ω/km
Line inductance	1 mH/km
Line length	5 km

Table 8: System and line characteristics

Bolted three-phase faults at 10 different positions along the transmission line have been simulated. These positions range from 0,1 to 1 per unit (p.u.) of the line's total length. This way, each fault was introduced at specific locations along the line, ensuring homogeneous coverage. This approach makes it easy to evaluate the performance of the distance protection element, as it must be able to identify whether a fault is within the protected zone or not. For each position, multiple values of the SIR (SCP) of the nearby bus and two different point on wave values have been used.

Table 9 lists the different SIR values and their respective SCP values used for the simulations, the selected point on wave values are the *zero-crossing instant* and the *peak voltage instant*.

The element will be tested while keeping the SIR of the remote bus constant because, given that the faults resistance will be always null, it gives no contribution to the fault voltage and fault current of the nearby bus, therefore it does not affect the functionality of the element.

S_{sc} [MVA]	SIR
2500	0,1
500	0,5
250	1
100	2,4
50	5
10	24

Table 9: SIR and respective SCP used fo the simulations

The element settings used affect its performance (Section 4.4.3), so it is important to establish them and explain the reasons for these choices. Table 10 lists the TD21 element settings used during the simulations.

Parameter description	Value
Time delay of the IQ element	1 power cycle
Element reach	0,8 pu
Security factor	1
Minimum restraining level (MRL)	0 pu
Security band (SB)	0 ms
Security margin (SM)	variable

Table 10: TD21 settings

Because the implemented Simulink model does not account for measurement errors (e.g. it does not account relay measurement or measurement transformers errors) and the line is modelled as an RL impedance, the reach point voltage evaluated using (44) will be very accurate, therefore it is not necessary to utilize the Security factor, the Security band or the Minimum restraining level for security.

The security margin (SM), as discussed in Section 4.4.3, significantly affects the speed and reliability of the element. Moreover, the determination of its value is not provided in literature. For these reasons, different SM values will be considered in the simulations, and the performance of the element will be analysed based on the adopted SM. The chosen SM are: 5, 10, and 30.

The simulation results will show the intervention times (if the element has intervened), under the various conditions analysed (fault location, point on wave,

SIR and SM). It is important for the element to be able to respond only to faults located within the protected zone, i.e. within the reach point.

4.6.1 Simulation results

Tables 11, 12, 13, 14 and 15 report the intervention times of the TD21 element, depending on fault location, point on wave and SM, with the respective SIR (Table 9).

Figure 25 shows the average intervention time and the dependability curve of the implemented element as a function of the fault location, also showing the influence of the SM on its performance. From these results, the following conclusions can be drawn about the simulated element:

- The intervention time decreases as the SIR increases.
- The intervention time increases as it gets closer to the reach (0.8 pu in these simulations).
- The intervention time increases if the fault occurs near the zero-crossing of the voltage and decreases if it occurs near the peak.
- The higher the SM the lower the intervention time

These characteristics are consistent with the expected behaviour, described in Section 4.4.3.

To further investigate the effect of the SIR on the operation of the TD21, Figure **??** shows the value of the integral $\int(|\Delta v_r| - v_{rst})dt$ (45) as a function of fault location and SIR. To highlight the difference in the order of magnitude of the integral value as the SIR increases, the results of a simulation conducted with a very high SIR (80) are also shown in the figure.
In all the analysed cases, the element never intervenes if the fault is outside the protected zone. In fact the integral $\int(|\Delta v_r| - v_{rst})dt$ is always null for faults located above 0,7 pu length.

Element Validation

The implemented TD21 model is based on scientific articles and instruction manuals. However, these sources often omit details about the settings of certain parameters, making it impossible for the model to be perfectly accurate. The key point is that the model behaves as expected, which is true in this case. In fact the response times obtained and the dependability of the element are consistent with those reported in the scientific literature in [16] [17] [21].

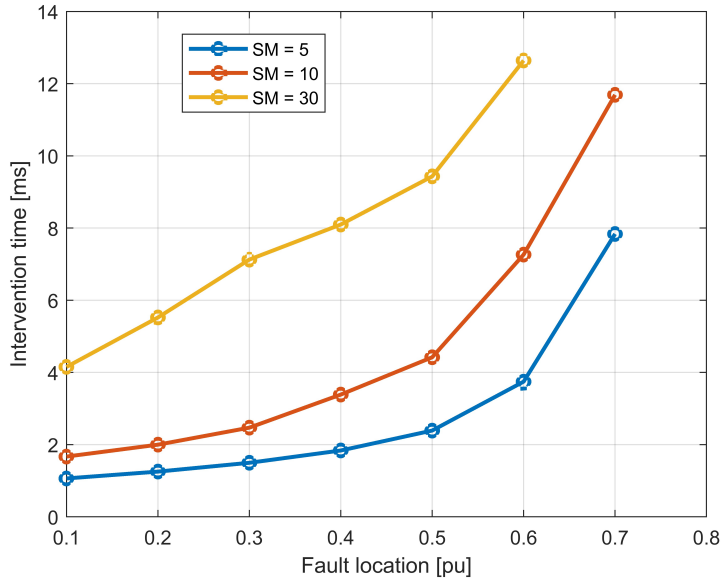

(a) Average intervention time as function of the fault location and SM

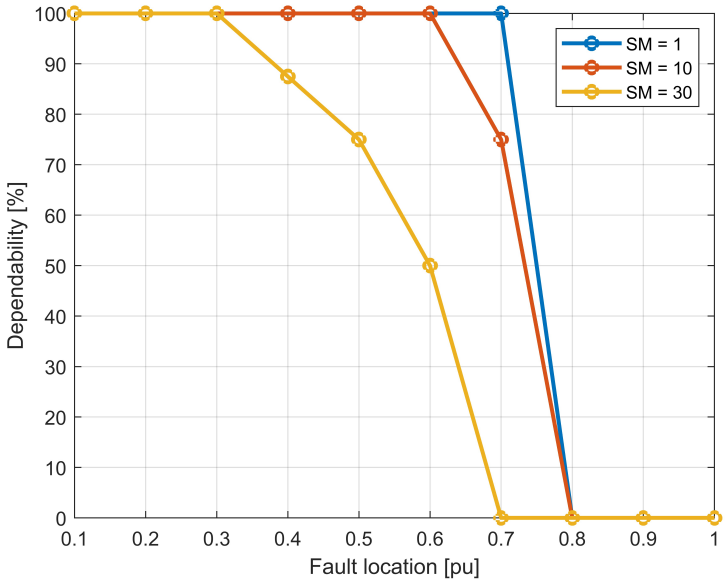

(b) Dependability curve as function of the fault location and SM

Figure 25

Fault location	SM = 5		SM = 10		SM = 30	
	zero-crossing	peak voltage	zero-crossing	peak voltage	zero-crossing	peak voltage
0.1	0.75	0.09	1.06	0.18	1.85	0.53
0.2	0.99	0.16	1.41	0.31	2.47	0.93
0.3	1.26	0.25	1.79	0.49	3.17	1.52
0.4	1.58	0.39	2.25	0.77	4.07	2.52
0.5	2.00	0.62	2.88	1.26	5.43	6.70
0.6	2.69	1.09	3.93	2.33	9.13	10.04
0.7	4.26	2.77	6.74	8.46	-	-
0.8	-	-	-	-	-	-
0.9	-	-	-	-	-	-
1	-	-	-	-	-	-

Table 11: Intervention time with SIR = 0,1 (2500 MVA)

Fault location	SM = 5		SM = 10		SM = 30	
	zero-crossing	peak voltage	zero-crossing	peak voltage	zero-crossing	peak voltage
0.1	1.30	0.27	1.84	0.53	3.24	1.60
0.2	1.52	0.36	2.15	0.72	3.84	2.24
0.3	1.78	0.50	2.54	0.99	4.61	3.36
0.4	2.12	0.70	3.04	1.40	5.71	7.35
0.5	2.60	1.03	3.76	2.15	7.79	9.70
0.6	3.40	1.74	5.05	4.57	15.24	16.15
0.7	5.37	6.59	11.86	10.95	-	-
0.8	-	-	-	-	-	-
0.9	-	-	-	-	-	-
1	-	-	-	-	-	-

Table 12: Intervention time with SIR = 0,5 (500 MVA)

Fault location	SM = 5		SM = 10		SM = 30	
	zero-crossing	peak voltage	zero-crossing	peak voltage	zero-crossing	peak voltage
0.1	1.76	0.49	2.50	0.97	4.50	3.16
0.2	1.99	0.62	2.84	1.23	5.20	5.60
0.3	2.27	0.80	3.26	1.62	6.19	8.20
0.4	2.66	1.08	3.84	2.24	7.88	9.99
0.5	3.20	1.56	4.71	3.54	14.08	12.88
0.6	4.15	2.63	6.38	8.37	-	-
0.7	6.70	8.72	15.43	16.69	-	-
0.8	-	-	-	-	-	-
0.9	-	-	-	-	-	-
1	-	-	-	-	-	-

Table 13: Intervention time with SIR = 1 (250 MVA)

Fault location	SM = 5		SM = 10		SM = 30	
	zero-crossing	peak voltage	zero-crossing	peak voltage	zero-crossing	peak voltage
0.1	2.72	1.14	3.93	2.36	7.99	10.37
0.2	3.01	1.39	4.37	2.96	12.13	11.77
0.3	3.38	1.74	4.97	4.10	15.13	14.84
0.4	3.88	2.30	5.84	7.71	19.15	-
0.5	4.66	3.44	7.39	9.68	-	-
0.6	6.12	8.14	14.27	13.21	-	-
0.7	14.55	13.74	-	-	-	-
0.8	-	-	-	-	-	-
0.9	-	-	-	-	-	-
1	-	-	-	-	-	-

Table 14: Intervention time with SIR = 2,4 (100 MVA)

Fault location	SM = 5		SM = 10		SM = 30	
	zero-crossing	peak voltage	zero-crossing	peak voltage	zero-crossing	peak voltage
0.1	3.88	2.31	5.81	7.75	19.44	-
0.2	4.27	2.84	6.53	8.85	-	-
0.3	4.79	3.73	7.65	10.05	-	-
0.4	5.56	7.21	12.18	11.80	-	-
0.5	6.83	9.18	16.13	18.11	-	-
0.6	12.94	12.15	-	-	-	-
0.7	-	-	-	-	-	-
0.8	-	-	-	-	-	-
0.9	-	-	-	-	-	-
1	-	-	-	-	-	-

Table 15: Intervention time with SIR = 5 (50 MVA)

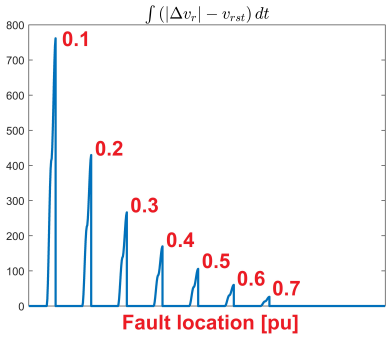

(a) SIR = 0.1

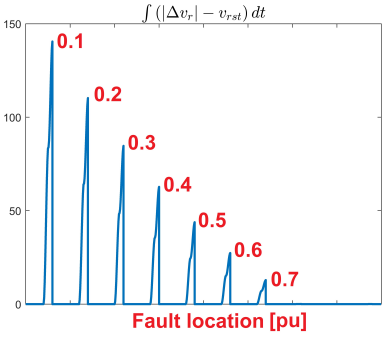

(b) SIR = 1

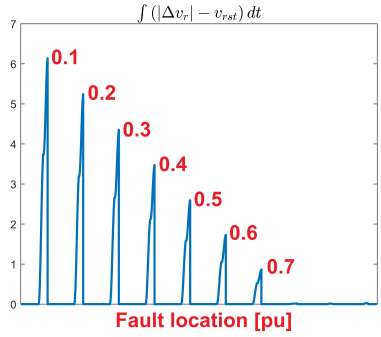

(c) SIR = 24

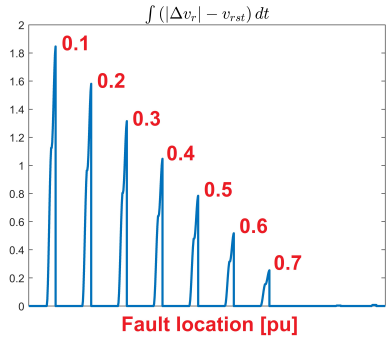

(d) SIR = 80

Figure 26: $\int (|\Delta v_r| - v_{rst})dt$ as a function of fault location and for different SIR

4.7 Unbalanced faults

As mentioned earlier the implemented TD21 element is capable of operating only on symmetrical three-phase faults, since these are the only faults that will be analysed in this thesis. However, the modifications needed to make the TD21 work in the presence of unbalanced faults are straightforward. In fact, it is sufficient to evaluate the reach point voltage (44) differently depending on the type of fault being monitored [19] [5].

Table 16 list the voltages and replica currents to be used in (44) depending on the fault type.

Fault type	Voltage v	Replica current i_z
AG	v_A	$i_{z_A} - i_{z_0}$
BG	v_B	$i_{z_B} - i_{z_0}$
CG	v_C	$i_{z_C} - i_{z_0}$
AB	$v_A - v_B$	$i_{z_A} - i_{z_B}$
BC	$v_B - v_C$	$i_{z_B} - i_{z_C}$
CA	$v_C - v_A$	$i_{z_C} - i_{z_A}$

Table 16: Loop voltages and currents

R_1, R_0, L_1, and L_0 are the resistance and inductance of the positive Z_1 and zero Z_0 sequence line impedances. i_{z_0} is the zero sequence replica current:

$$i_0 = \frac{i_A + i_B + i_C}{3} \tag{51}$$

$$i_{z_0} = \frac{R_1}{Z_1} i_0 + \frac{L_1}{Z_1} \frac{di_0}{dt} - \frac{Z_0}{Z_1} \left(\frac{R_0}{Z_0} i_0 + \frac{L_0}{Z_0} \frac{di_0}{dt} \right) \tag{52}$$

Example

For example, in the case of a phase-to-ground fault involving phase A:

$$i_{z_A} = \frac{R_1}{Z_1} i_A + \frac{L_1}{Z_1} \frac{di_A}{dt} \tag{53}$$

$$i_{z_{AG}} = i_{z_A} - i_{z_0} \tag{54}$$

$$v_{AG} = v_A \tag{55}$$

$$v_r = v_{AG} - m_0 \cdot i_{z_{AG}} \cdot Z_1 \tag{56}$$

5 Case study: VSC connected to a line protected with the TD21 element

5.1 Introduction

In this chapter the results of the simulations performed using the software MATLAB/Simulink are presented and discussed. The simulations are designed to evaluate the impact of the implemented VSC converter, described in Section 3, fault behaviour on the TD21 distance protection element, described in Section 4.

The setup of the simulation is shown in Figure 27: the VSC converter is connected, via a transformer, to a line protected by the TD21 element. The parameters of the VSC and LCL filter are the same as those presented in Section 3.8, Table 2 and 3. The TD21 element settings are the same as those presented in Section 4.6, Table 10. The line is represented by an RL impedance, and the transformer is modelled as an inductance. The line, transformer, and grid parameters are detailed in Table 17. The circuit is simulated with all elements (transformer, line, and grid) represented on the low voltage side.

Similar to the simulations conducted to test the TD21 element in Section 4.6, faults are simulated along the entire length of the line: 10 different bolted three-phase faults at different positions; these positions range from 0,1 to 1 per unit (p.u.) of the line's total length.

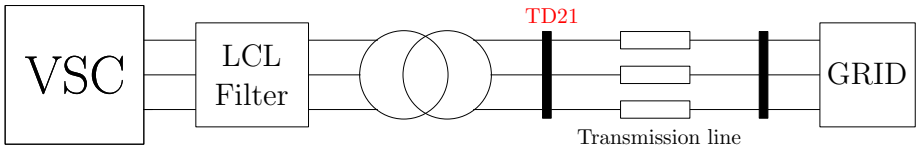

Figure 27: Network used for the simulations

Line	
Line resistance	0,1 Ω/km
Line inductance	1 mH/km
Line length	5 km
Transformer	
Rated voltage	400 V / 20 kV
Rated power	120 kVA
Short circuit voltage	5 %
Grid	
Short circuit power	100 MVA
$\frac{X}{R}$	10

Table 17: Line, transformer and grid parameters

5.2 Simulation results

During the simulations, two issues emerged:

- Limited Fault Current: The fault current provided by the VSC is limited, which reduces the effectiveness of the TD21. For short lines, this limitation might result in the TD21 not operating correctly for faults within the protected zone. In fact low integral values cause the TD21 to intervene only if the Security Margin (SM) is sufficiently low. However, in a real world scenario a low SM can lead to incorrect fault detection due to the influence of measurement errors in the sensor chain (instrument transformer errors and relay measurement errors).

- Irregular Fault Current During Transient Response: During the transient response of the VSC control system (ICC and PLL specifically), the fault current is irregular and unpredictable, differing significantly from the fault current of traditional synchronous generators. In traditional generators, the fault current is a combination of an exponential decay and a sinusoidal component. In contrast, the VSC's fault current during the transient phase affects the accuracy of the voltage assessment at the reach point (44), causing it to operate even for faults outside the protected zone.

These issues are illustrated in Figure 28, which shows the value of the integral $\int(|\Delta v_r| - v_{rst})dt$ (45) as a function of the fault position. The figure indicates that the integral value is very low compared to the one evaluated in the presence of traditional generators, as shown in Section 4.6.1. For comparison, these values are also shown in Figure 29. Furthermore, the integral value is non-zero even for faults outside the protected zone (beyond 0,8 pu), leading to undesired operation of the protection element.

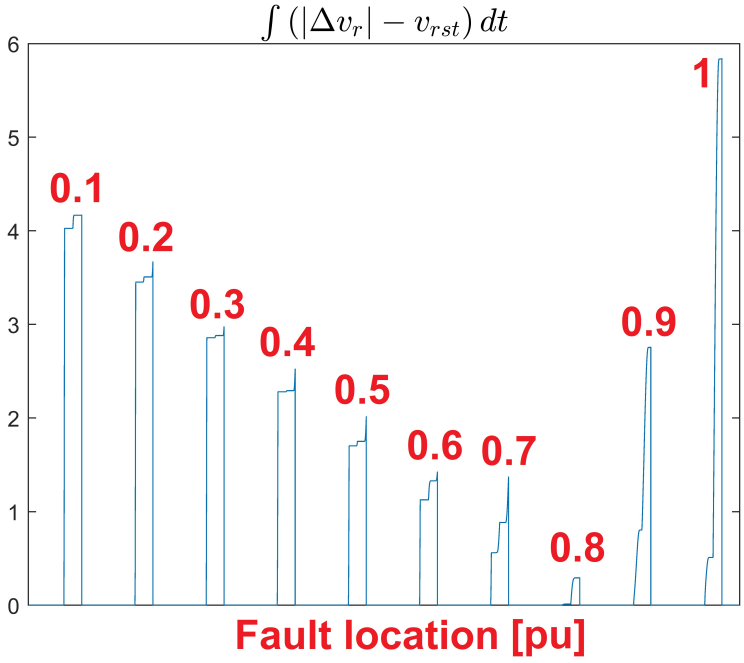

Figure 28: $\int(|\Delta v_r| - v_{rst})dt$ as a function of fault location

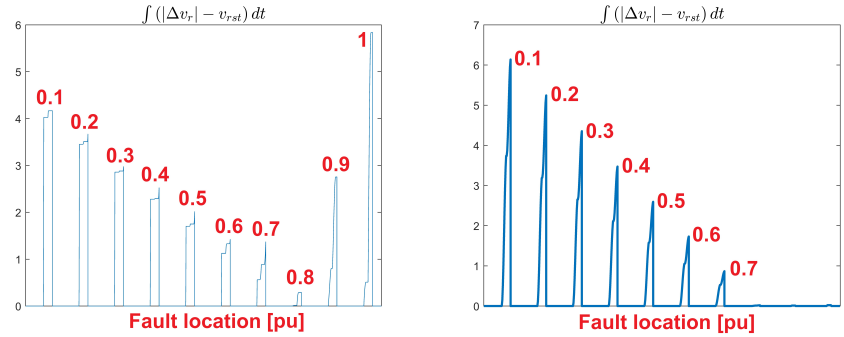

(a) VSC

(b) SIR = 24

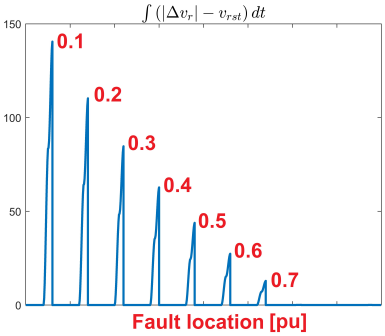

(c) SIR = 1

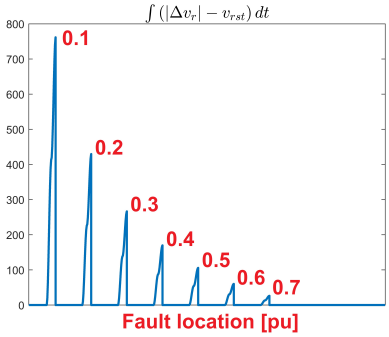

(d) SIR = 0.1

Figure 29: $\int (|\Delta v_r| - v_{rst})dt$ as a function of fault location

6 Conclusions and Future work

The objective of this thesis was to analyse the impact of fault current injection by power electronic converters (PECs), specifically voltage source converters (VSCs), on incremental quantities (IQ) based distance protection, particularly the TD21 distance protection element, incorporated in the SEL-T400L relay. To achieve this, several key tasks were undertaken, including a literature review on PECs fault behaviour, the implementation of VSC and TD21 models in MATLAB/Simulink, and the evaluation of the VSC's fault behaviour on the TD21 element.

The VSC model was successfully implemented, using the German grid code requirements on Fast Fault Current Injection (FFCI) for the converter's fault behaviour, as detailed in Chapter 3. This model was designed to replicate the behaviour of VSCs under both normal and fault conditions. Similarly, the TD21 distance protection element was successfully implemented based on scientific literature and its specific manual, designed to detect and clear faults using incremental quantities, as detailed in Chapter 4. The influence of VSC fault behaviour on the TD21 element was evaluated through simulations performed in MATLAB/Simulink, as detailed in Chapter 5. These simulations were crucial in understanding how the unique characteristics of VSC fault currents impact the performance of the TD21 protection scheme.

The simulations revealed that the limited fault current provided by the VSC poses a significant challenge for distance protection schemes like the TD21. This reduced fault current can hinder the ability of the protection element to detect and clear in-zone faults effectively, with the issue worsening as the line length decreases. Additionally, the irregular and unpredictable transient response of the VSC's fault current, very different from the fault current characteristics of traditional synchronous generators, affects the accuracy of the voltage assessment at the reach point, causing the TD21 element to operate for faults outside the protected zone.

The results of this study underscore the challenges posed by the integration of VSCs, and in general PECs, in modern power systems, particularly concerning protection schemes. The low fault current and the unpredictable nature of VSC fault currents during transient responses pose significant challenges for both traditional and new time-domain protection schemes like the TD21. These findings highlight the importance of adapting protection schemes to accommodate the unique behaviour of PECs during faults. Future work should focus on exploring more detailed scenarios, including asymmetrical faults and more complex network configurations, to build upon the foundational insights provided by this study. By addressing these challenges, the reliability and stability of power systems with high integration of PECs can be ensured.

References

[1] Commission Regulation (EU) 2016/1447 of 26 August 2016 establishing a network code on requirements for grid connection of high voltage direct current systems and direct current-connected power park modules (Text with EEA relevance).

[2] Commission Regulation (EU) 2016/631 of 14 April 2016 establishing a network code on requirements for grid connection of generators (Text with EEA relevance).

[3] IEEE Guide for Protective Relay Applications to Transmission Lines. pages 1–141.

[4] Massive InteGRATion of power Electronic devices — MIGRATE Project — Fact Sheet — H2020 [https://cordis.europa.eu/project/id/691800].

[5] SEL-T400L Time-Domain Line Protection - Documentation.

[6] Nathan Baeckeland, Bert Herteleer, and Michael Kleemann. Modelling fault behaviour of power electronic converters.

[7] Chandra Bajracharya. Control of VSC-HVDC for wind power.

[8] Holger Berndt. TransmissionCode 2007 Network and System Rules of the German Transmission System Operators VDN.

[9] M. Chamia and S. Liberman. Ultra High Speed Relay for EHV/UHV Transmission Lines – Development, Design and Application. PAS-97(6):2104–2116.

[10] Ali Hooshyar, Maher A. Azzouz, and Ehab F. El-Saadany. Distance Protection of Lines Emanating From Full-Scale Converter-Interfaced Renewable Energy Power Plants—Part I: Problem Statement. 30(4):1770–1780.

[11] B. Kasztenny. Line distance protection near unconventional energy sources. In *16th International Conference on Developments in Power System Protection (DPSP 2022)*, volume 2022, pages 224–229.

[12] Bogdan Kasztenny, Armando Guzman, Normann Fischer, Mangapathirao Mynam, and Douglas Taylor. Practical Setting Considerations for Protective Relays That Use Incremental Quantities and Traveling Waves.

[13] S. Rüberg and V. Sewdien. Deliverable D1.6 Demonstration of Mitigation Measures and Clarification of Unclear Grid Code Requirements.

[14] Fahmid Sadeque, Md. Shamim Reza, and Md Maruf Hossain. Three-Phase Phase-Locked Loop for Grid Voltage Phase Estimation under Unbalanced and Distorted Conditions. pages 1–7.

[15] Marwa Saïd-Romdhane, M.W. Naouar, Ilhem Slama-Belkhodja, and E. Monmasson. Simple and systematic LCL filter design for three-phase grid-connected power converters. 130.

[16] Edmund Schweitzer, Bogdan Kasztenny, and Mangapathirao Mynam. Performance of time-domain line protection elements on real-world faults. pages 1–17.

[17] Edmund Schweitzer, Bogdan Kasztenny, Mangapathirao Mynam, Armando Guzman, Normann Fischer, and Veselin Skendzic. Defining and Measuring the Performance of Line Protective Relays.

[18] Edmund O. Schweitzer and Bogdan Kasztenny. Distance protection: Why have we started with a circle, does it matter, and what else is out there? In *2018 71st Annual Conference for Protective Relay Engineers (CPRE)*, pages 1–19.

[19] Edmund O. Schweitzer, Bogdan Kasztenny, Armando Guzmán, Veselin Skendzic, and Mangapathirao V. Mynam. Speed of line protection - can we break free of phasor limitations? In *2015 68th Annual Conference for Protective Relay Engineers*, pages 448–461.

[20] A N R L Sirisha and S. R. Bhide. Incremental quantities based relays. In *2014 International Conference on Power, Automation and Communication (INPAC)*, pages 27–32.

[21] Danillo de Oliveira Sobreira and Aryfrance Rocha Almeida. Protection of Transmission Lines in the Time Domain Using Incremental Quantities with Atp/Atpdraw.

[22] Mads Graungaard Taul, Xiongfei Wang, Pooya Davari, and Frede Blaabjerg. Grid Synchronization of Wind Turbines during Severe Symmetrical Faults with Phase Jumps. In *2018 IEEE Energy Conversion Congress and Exposition (ECCE)*, pages 38–45.

[23] Mads Graungaard Taul, Xiongfei Wang, Pooya Davari, and Frede Blaabjerg. An Overview of Assessment Methods for Synchronization Stability of Grid-Connected Converters Under Severe Symmetrical Grid Faults. 34(10):9655–9670.

[24] Remus Teodorescu, Marco Liserre, and Pedro Rodr´ıguez. *Grid Converters for Photovoltaic and Wind Power Systems.*

[25] Michael J. Thompson and Amit Somani. A tutorial on calculating source impedance ratios for determining line length. In *2015 68th Annual Conference for Protective Relay Engineers*, pages 833–841.

[26] J. Wang, Y. Li, and F. Hohn. Impact and challenges of conventional protection solutions in wind farm connected grids. In *16th International Conference on Developments in Power System Protection (DPSP 2022)*, volume 2022, pages 230–237.

[27] Jialiang Wu, Zhen Wang, Hong Rao, Yijing Chen, and Weihuang Huang. A Review of Control Strategies for Inertia Support in VSC-HVDC System. In *2019 4th IEEE Workshop on the Electronic Grid (eGRID)*, pages 1–6.